Electron Transfer and Protein Dynamics in the Photosynthetic Reaction Center

Benjamin H. McMahon,* Joachim D. Müller,* Colin A. Wraight,#§ and G. Ulrich Nienhaus*§¶
*Departments of Physics and #Plant Biology, and §Center for Biophysics and Computational Biology, University of Illinois at Urbana-Champaign, Urbana, Illinois 61801 USA, and ¶Department of Biophysics, University of Ulm, D-89069 Ulm, Germany

ABSTRACT We have measured the kinetics of electron transfer (ET) from the primary quinone (Q_A) to the special pair (P) of the reaction center (RC) complex from *Rhodobacter sphaeroides* as a function of temperature (5–300 K), illumination protocol (cooled in the dark and under illumination from 110, 160, 180, and 280 K), and warming rate (1.3 and 13 mK/s). The nonexponential kinetics are interpreted with a quantum-mechanical ET model (Fermi's golden rule and the spin-boson model), in which heterogeneity of the protein ensemble, relaxations, and fluctuations are cast into a single coordinate that relaxes monotonically and is sensitive to all types of relaxations caused by ET. Our analysis shows that the structural changes that occur in response to ET decrease the free energy gap between donor and acceptor states by 120 meV and decrease the electronic coupling between donor and acceptor states from 2.7×10^{-4} cm^{-1} to 1.8×10^{-4} cm^{-1}. At cryogenic temperatures, conformational changes can be slowed or completely arrested, allowing us to monitor relaxations on the annealing time scale ($\sim 10^3$–10^4 s) as well as the time scale of ET ($\sim$100 ms). The relaxations occur within four broad tiers of conformational substates with average apparent Arrhenius activation enthalpies of 17, 50, 78, and 110 kJ/mol and preexponential factors of 10^{13}, 10^{15}, 10^{21}, and 10^{25} s^{-1}, respectively. The parameterization provides a prediction of the time course of relaxations at all temperatures. At 300 K, relaxations are expected to occur from 1 ps to 1 ms, whereas at lower temperatures, even broader distributions of relaxation times are expected. The weak dependence of the ET rate on both temperature and protein conformation, together with the possibility of modeling heterogeneity and dynamics with a single conformational coordinate, make RC a useful model system for probing the dynamics of conformational changes in proteins.

INTRODUCTION

Proteins exhibit substantial variability around the average structure, as determined, for instance, by x-ray crystallography (Frauenfelder et al., 1979; Hartmann et al., 1982). This is because proteins do not possess a unique state of minimum free energy, but assume a large number of conformational substates (CSs) that can be represented by nearly isoenergetic local minima in a complex energy landscape, separated by free energy barriers that have to be surmounted during a conformational change (Frauenfelder and Wolynes, 1994). In the energy landscape, the CSs are grouped in tiers that can be characterized by markedly different apparent activation energies. Because the barriers differ widely in height, protein motions are characterized by time scales ranging over many orders of magnitude (Young et al., 1991; Jackson et al., 1994; Green et al., 1994; Johnson et al., 1996).

In proteins, conformational dynamics is intimately connected to function. Rates of reactions can be governed by the time it takes for the protein to fluctuate into a reactive conformation, and the transfer of a substrate molecule to an active site requires commensurate structural adaptations of the protein. Temperature-dependent studies of protein reactions reveal energetic aspects of the conformational changes that accompany the reaction. At low temperatures, many degrees of freedom are thermally arrested, and distributions of reaction rates reflect the heterogeneity of the ensemble of protein molecules frozen in different CSs. At intermediate temperatures, conformational transitions occur on the time scale of the reaction, which allows one to investigate protein motions through studies of reaction kinetics. At sufficiently high temperatures, each protein molecule fluctuates among the CSs on time scales shorter than that of the reaction, and kinetic averaging leads to single-valued rate coefficients. This interplay between protein dynamics and biological function has been studied extensively in ligand binding to heme proteins (Austin et al., 1975; Agmon and Hopfield, 1983; Steinbach et al., 1991; Nienhaus et al., 1992; Ansari et al., 1994; Agmon et al., 1994; Panchenko et al., 1995).

In this paper we have investigated the coupling of protein motions to long-range electron transfer (ET) in reaction centers (RCs) of purple bacteria (*Rhodobacter sphaeroides*). In these bacteria, the photon energy absorbed by light-harvesting complexes or RC cofactors is transferred to the special pair (P), a bacteriochlorophyll dimer on the periplasmic side of the RC protein, and the electronic system is promoted to the first excited singlet state, P*. An electron is subsequently transferred from P* to a bacteriopheophytin (H) and further to the primary quinone (Q_A), located 25 Å away from the special pair, closer to the cytoplasmic side of the protein (Allen et al., 1987). In the absence of the secondary quinone (Q_B), the electron then recombines with the hole on the special pair, and the RC is

Received for publication 1 August 1997 and in final form 21 January 1998.
Address reprint requests to Dr. Gerd Ulrich Nienhaus, Abteilung Biophysik, Universität Ulm, Albert-Einstein-Allee 11, 89081 Ulm, Germany. Tel.: 49-731-502-3050; Fax: 49-731-502-3059; E-mail: uli@uiuc.edu.

0006-3495/98/05/2567/21 $2.00

restored to the ground state:

$$PH_AQ_A + h\nu \rightarrow P^*H_AQ_A \rightarrow P^+H_A^-Q_A \rightarrow P^+H_AQ_A^- \rightarrow PH_AQ_A. \quad (1)$$

The charge separation during this cycle is a substantial perturbation of the protein that results in conformational changes that influence the ET rate, as has been noted in previous studies of the "preillumination" effect and of delayed fluorescence (Noks et al., 1977; Kleinfeld et al., 1984; Woodbury and Parson, 1986; Rubin et al., 1994; Peloquin et al., 1994). These changes can be studied conveniently in this system because the reaction is initiated by light, can be followed spectroscopically, and is completed on the millisecond time scale.

We have investigated the last and slowest ET step in the sequence, $P^+Q_A^- \rightarrow PQ_A$ (because the pheophytin is not involved in this particular ET step, we drop the H for simplicity), by measuring its ET kinetics at temperatures from 5 to 300 K, and examined the influence of illumination on the ET kinetics by switching on a strong light source during cooling at various temperatures T_L to keep the protein in the charge-separated state. The experiments give clear evidence that, after light-induced charge separation at high temperature, the protein relaxes from a dark-adapted conformation to a light-adapted conformation that can be trapped by cooling to low temperature. We probe these conformational changes through their effect on the ET kinetics.

The $P^+Q_A^- \rightarrow PQ_A$ ET is long-ranged, and the large spatial separation leads to weak coupling of the donor and acceptor electronic states, which ensures nonadiabatic ET from a thermally equilibrated initial manifold of vibrational states. We use the spin-boson model (SBM) (Leggett et al., 1987; Warshel et al., 1989; Xu and Schulten, 1994) to describe the ET kinetics as a function of temperature in terms of the underlying physical quantities, introducing a distribution of energy gaps and electronic coupling between the donor and acceptor states to account for the structural heterogeneity in the sample. The analysis follows the dissipation of energy over a wide range in time and temperature, as the RC adapts to the change in charge distribution due to ET. The results complement relaxation studies in heme proteins and are likely to be of importance in understanding relaxation processes in proteins in general.

EXPERIMENTAL PROCEDURES

Reaction centers were freshly prepared from *Rhodobacter sphaeroides* (Maróti and Wraight, 1988), and the quinones were extracted to less than 1% Q_B. The protein solution in 0.1% LDAO, 1 mM Tris buffer (pH 8) was mixed with glycerol (75%, v/v). The sample was loaded in a $10 \times 10 \times 2.5$ mm^3 plastic cuvette that was in thermal contact with a copper sample holder in a storage cryostat (model 10-DT; Janis Research Co., Wilmington, MA). A digital temperature controller (model DRC 82C; Lake Shore Cryotronics, Westerville, OH) was used to adjust the temperature to within ± 0.3 K.

Photoinitiation of the electron transfer cycle was accomplished with a 6-ns (full width at half maximum) pulse (532 nm, 80 mJ) from a frequency-doubled, Q-switched Nd-YAG laser (model NY-61; Continuum, Santa Clara, CA). Optical absorbance changes were monitored with light from a tungsten lamp that was passed through a monochromator set at 435 nm. The light intensity was measured with a photomultiplier tube (model R 928; Hamamatsu Corp., Middlesex, NJ) and digitized with a 500-MHz digital storage oscilloscope from 30 ns to 100 μs (model TDS 520; Tektronix, Wilsonville, OR) and a home-made logarithmic time-base digitizer (Wondertoy II) (Berendzen et al., 1989) from 2 μs to 1000 s. For a single transient, the noise was $\sim$200 μOD on the millisecond time scale.

The loaded RC samples were cooled at a rate of $\sim$20 K/min until the sample cuvette was immersed in liquid helium (4.2 K). To cool under illumination, light from a 250-W tungsten lamp (Oriel), filtered with an IR heat filter and a 650-nm long pass filter, was switched on at different temperatures T_L. With this setup, an excitation rate k_L of the RC molecules of $\sim$200 s^{-1} was achieved, as determined by measurement of the flash-induced signal amplitude with and without continuous background illumination. (The measured signal decreased by 85% upon illumination at 80 K, where the average electron transfer rate is 40 s^{-1}.)

After cooling either under light or in the dark, the sample was warmed in the dark at a rate of 1.3 or 13 mK/s. The ET kinetics were measured at fixed temperature intervals, with $\sim$5 min of equilibration time at each temperature and between flashes. For the measurement where the sample was cooled in the dark, five traces were averaged at each temperature. In the experiments where the sample was cooled under illumination, either 3 or 15 traces (depending on the warming rate) were averaged at each temperature.

RESULTS

Fig. 1 shows measurements of the $P^+Q_A^- \rightarrow PQ_A$ ET kinetics for various temperatures between 5 and 280 K. Small amounts ($\sim$15% of total amplitude) of an interfering process occur on the 100-μs time scale, arising from the decay of the triplet state of the special pair. (The triplet signal arises from a small population of RCs lacking Q_A, an inevitable consequence of Q_B depletion.) However, this process can be easily separated because it is well represented by a single exponential, so that the $P^+Q_A^- \rightarrow PQ_A$ kinetics were accurately determined.

For the data plotted with diamonds in Fig. 1, *a* and *b*, the sample was cooled in the dark. Subsequently, the temperature was increased in a stepwise fashion, and the kinetics were measured in 5-K intervals. For clarity, we show only data for 5, 60, 120, and 160 K in Fig. 1 *a*, and 200 and 280 K in Fig. 1 *b*. The solid and dashed lines are fits with a model that will be described in the following section.

The triangles represent data taken with the same sample after cooling under illumination from $T_L = 280$ K. With the excitation rate $k_L \approx 200$ s^{-1} and an average recombination rate of $\sim$10 s^{-1}, illumination keeps the proteins in the charge-separated state $\sim$95% of the time. From the comparison of the two data sets (particular in Fig. 1 *a*), it is obvious that illumination traps the protein in a conformation different from that obtained when it is cooled in the dark. These differences persist as the protein is warmed in the dark. At higher temperatures, the difference in ET kinetics becomes successively smaller, demonstrating that the changes are reversible. The significant loss in signal amplitude upon cooling under illumination, mentioned in the

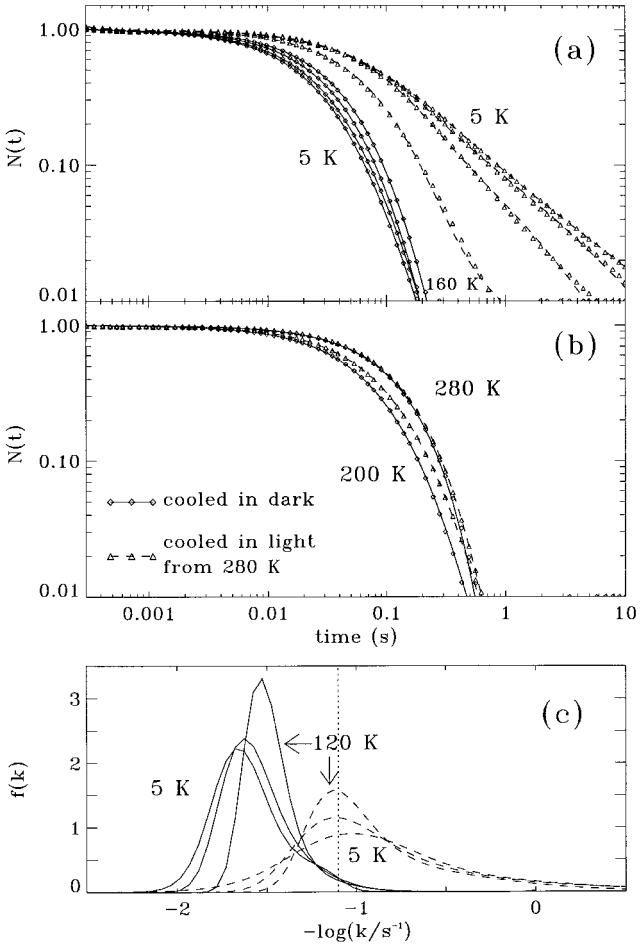

FIGURE 1 Normalized absorbance changes at 435 nm, $N(t)$, representing $P^+Q_A^- \rightarrow PQ_A$ electron transfer at (*a*) 5, 60, 120, 160 K and (*b*) 200 and 280 K for reaction center samples cooled in the dark (◇), and samples cooled under illumination from 280 K (△). The lines are fits with the ET model described in text. The absorbance difference at 435 nm (1 ms) was, in order of increasing temperature, 510, 525, 542, 537, 503, and 503 mOD for the dark-cooled sample, and 286, 263, 256, 279, 281, and 444 mOD for the light-cooled sample. (*c*) Rate distributions, $f(k)$, of the 5, 60, and 120 K kinetics shown in *a*, calculated with the maximum entropy method for the dark-cooled (—) and light-cooled (– – –) samples. The dotted line indicates the isokinetic point; larger ET rates increase with temperature, and smaller ET rates decrease.

figure caption, recovers between 250 and 300 K. Because the return of signal occurs at a distinctly higher temperature than the other motions we observe, we expect it to be an unrelated process that affects only the signal amplitude.

Only at the highest temperatures ($T > 260$ K) can the $P^+Q_A^- \rightarrow PQ_A$ ET be adequately described by a single exponential. Because the kinetics are nonexponential at lower temperatures, they carry more information than just a single rate coefficient for the electron transfer. No evidence exists for a particular decomposition into multiple discrete processes (note, especially, the breadth and smoothness of the curve measured at 5 K after cooling in light, Fig. 1 *a*). Therefore, we describe the kinetics, $N(t)$, with a rate distribution function, $f(k)$, defined on a logarithmic scale (Steinbach et al., 1992),

$$N(t) = \int f(k) \exp(-kt) d \log k. \quad (2)$$

In Fig. 1 *c*, rate distributions are shown for 5, 60, and 120 K that were calculated with the maximum entropy method (MEM) (Steinbach et al., 1992). The slowing of the kinetics with increasing temperature, observed after cooling in the dark, is reflected by a shift of the rate distributions to slower rates. For the sample cooled under illumination, $f(k)$ narrows with increasing temperature, shifting slightly. An interesting feature of the rate distributions, both for cooling in the dark and under light, is that, for populations with $k > 12$ s^{-1}, ET slows with increasing temperature, whereas the opposite temperature dependence is observed for those RCs with $k < 12$ s^{-1}. This is evident because the area of the distribution with $k > 12$ s^{-1} is temperature independent. In the next section, this behavior will be explained by our ET model, which predicts an isokinetic point, i.e., temperature-independent kinetics, for molecules in conformations having a rate coefficient $k = 12$ s^{-1}. We indicate this rate with a dotted line in Fig. 1 *c*.

A model-independent characterization of the rate distributions is provided by an average rate, k_{ET}, defined by

$$\log k_{ET} = \int f(k) \log k \, d \log k, \quad (3)$$

and the standard deviation, σ_k, of the distribution

$$\sigma_k = \sqrt{\int f(k)(\log k - \log k_{ET})^2 \, d \log k}. \quad (4)$$

Fig. 2 shows average rate coefficients (k_{ET}) and widths (σ_k) of the distributions that were calculated from the kinetic data of the RC sample cooled in the dark (*diamonds*) and cooled under illumination from various temperatures (110, 160, 180, and 280 K). It has long been known that, when RC samples are cooled in the dark, the recombination process is slowest at room temperature and speeds up severalfold as the temperature is lowered to 5 K (Parson, 1967). As shown in Fig. 2 *a*, the major part of this acceleration occurs over a 50-K window from 225 to 175 K. The steepness of this temperature dependence is not accounted for by any simple theoretical descriptions of electron transfer without allowing for independent and sometimes ad hoc temperature dependences of multiple model parameters.

RCs cooled under light from 280 K display ET kinetics markedly different from those of the dark-adapted sample (Figs. 1 and 2, *triangles*). At low temperatures ($T < 125$ K), the average rate coefficient (~6 s^{-1}) is similar to that seen at room temperature. However, as the sample is rewarmed in the dark, the recombination process accelerates to a maximum at ~175 K. Thereafter, it follows a pattern similar to that of the dark-adapted sample.

By comparing the ET rates for RCs cooled in the dark with those for RCs cooled under illumination, relaxation of

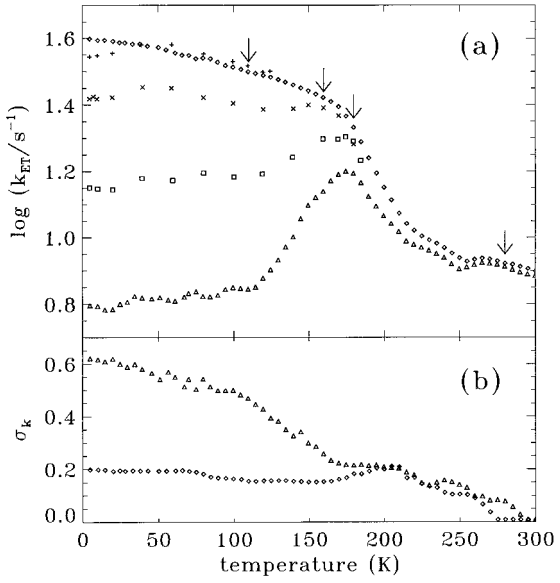

FIGURE 2 (*a*) Logarithm of the average rate coefficients of electron transfer (Eq. 3), measured while warming in the dark after cooling under illumination from 280 (△), 180 (□), 160 (×), 110 K (+) and in the dark (◇), using the rate distribution resulting from the best fit single Gaussian energy distribution, except for the measurements after cooling in light from 280 K. For the latter, fits between 5 and 175 K used a two-Gaussian energy distribution. Arrows indicate T_L, the temperature at which illumination began during cooling. ET rates for T_L = 110, 160, 180 K were acquired on a sample with ~60% Q_B; dark-cooled ET rates in this sample were slightly different from the data that are shown. Direct comparison of ET kinetics at T_L, before and after cooling under illumination (data not shown), revealed no irreversible changes. (*b*) Widths (in decades) of the rate distribution fits for the sample cooled under illumination from 280 K (△) and the sample cooled in the dark (◇).

the protein conformation on the time scale of warming (hours) can be monitored. There is a broad temperature range, primarily between 120 and 200 K, in which conformational changes are trapped and annealed. These changes anneal at or below T_L, the temperature at which cooling under illumination started. Evidently, proteins in conformations adapted to charge separation have a slower $P^+Q_A^- \rightarrow PQ_A$ process than those cooled in the dark, regardless of the temperature at which the adaptation occurs.

Several observations and inferences suggest that the step in k_{ET} of the dark-adapted sample, centered around 200 K in Fig. 2 *a*, originates from conformational changes of the protein:

1. The slow annealing of conformational changes observed between 120 and 200 K requires that they be visible on faster time scales at higher temperatures. After charge separation, the protein starts to relax toward the conformations that are adapted to the charge-separated state, which has the slower ET kinetics. Below 170 K, it relaxes only to a small extent during the 100 ms that charge separation persists. Above 170 K, appreciable relaxation occurs, and above 240 K, most of the relaxation is completed during the lifetime of the charge-separated state. Thus, at sufficiently high temperature, charge recombination occurs in a protein that is adapted to charge separation.

2. The glass transition temperature of the solvent used in these studies (3/1 glycerol/water, v/v) is 175 K. Above this temperature, solvent motions occur on time scales faster than 100 s (Huck et al., 1988), enabling major conformational rearrangements in the reaction centers. Studies of ligand binding to myoglobin in many different solvents indicate that protein dynamics is coupled to solvent viscosity (Beece et al., 1980; Ansari et al., 1994).

3. The behavior of the widths of the rate distributions also suggests a dynamic origin for the step in the ET rates. Below 170 K, nonexponential kinetics reflect mostly static heterogeneity of the proteins frozen in various conformations. Between 170 and 230 K, molecules that recombine quickly do so from a dark-adapted conformation with its high return rate, whereas proteins that recombine more slowly will have already evolved into a conformation that is more adapted to the charge-separated state, with its slower ET kinetics. The resulting time-dependent rate coefficient leads to additional broadening of the nonexponential kinetics, as seen in Fig. 2 *b* around 200 K. Above 210 K, the rate distribution begins to narrow because conformational fluctuations allow each protein molecule to visit many different CSs during the lifetime of the charge-separated state, so that ET occurs at an averaged rate. Fluctuational averaging of a particular motion is observed at a slightly higher temperature than the onset of the corresponding relaxation.

We used two different experimental approaches to measure conformational relaxation on widely separated time scales. To obtain data on long time scales (10^3 and 10^4 s), we observed the change in the kinetics as the light-cooled sample was slowly warmed in the dark, indicating relaxation of the cryogenically trapped light-adapted state toward the dark-adapted state. Relaxation on short time scales was determined from the behavior of the dark-cooled sample, indicating the extent of adaptation to charge separation in the ~100 ms between charge separation and recombination. A proper description of these qualitative observations requires a model of electron transfer that will allow a quantitative description of static heterogeneity, time-dependent rate coefficients, and fluctuational averaging at the various temperatures and conformations produced by cooling under illumination. A suitable model will be developed in the following section. It provides a mapping of our observable, the $P^+Q_A^- \rightarrow PQ_A$ electron transfer rate, onto a single physical parameter, ϵ, which represents the energy gap between $P^+Q_A^-$ and PQ_A and describes the conformation of the protein. The relation between the ET rate, *k*, and ϵ is plotted in Fig. 3 *a* for several temperatures. Those readers willing to accept our ET model are welcome to skip the following section.

QUANTITATIVE MODEL OF ELECTRON TRANSFER

Description

A simple theoretical description of the rate coefficient for nonadiabatic electron transfer is given by Fermi's golden

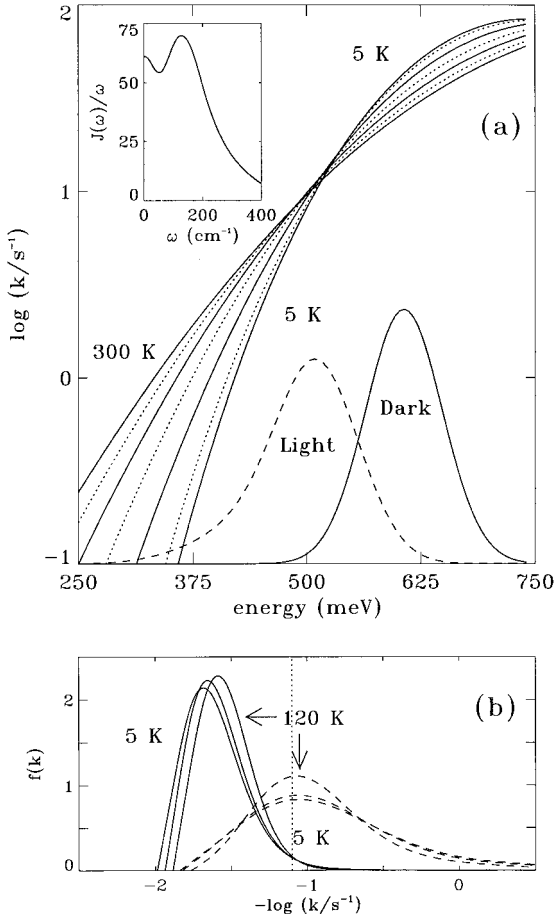

FIGURE 3 (*a*) Calculated electron transfer rates, $k(\epsilon, T)$, at 5, 50, 100, 150, 200, 250, and 300 K used to convert rate distributions $f(k)$ into energy gap distributions, $g(\epsilon)$. Included in the calculation is a linear dependence of the logarithm of the matrix element V on ϵ (Eq. 13). Also shown are the ϵ distributions needed to fit the 5-K ET kinetics of RC cooled in the dark and under illumination from $T_L = 280$ K. (*Inset*) Spectral density used in this calculation. Equation 6 was numerically integrated at 11 energies and 8 temperatures, and log k versus ϵ and T was interpolated with a cubic polynomial for intermediate values. Parameters used in the calculation are given in Table 1. (*b*) Rate distributions, $f(k)$, resulting from the energy gap distributions and the $k(\epsilon, T)$ shown in *a* for 5, 60, and 120 K.

rule and the Condon approximation (Levich and Dogonadze, 1959; Jortner, 1976; Closs and Miller, 1988),

$$k = \frac{2\pi}{\hbar} V^2 FC, \tag{5}$$

where $\hbar$ is Planck's constant divided by 2π, V is the electronic interaction matrix element that describes the weak coupling between the initial and final electronic states involved in the ET, and the thermally averaged Franck-Condon factor, FC, is a measure of the amount of overlap between the reactant and product nuclear wave functions.

To calculate FC, we use the spin-boson model (SBM), a simple quantum-mechanical description of ET coupled to a spectrum of harmonic oscillators (Garg et al., 1985; Leggett et al., 1987; Warshel et al., 1989; Xu and Schulten, 1994). It provides the temperature and energy gap dependence of FC in terms of $J(\omega)$, the vibrational density of states weighted by the (linear) coupling strength of each mode to the electronic transition:

$$FC(\epsilon, T) = \left(\frac{2}{\pi\hbar}\right)\int_0^\infty dt \cos\left(\frac{\epsilon t}{\hbar}\right)\cos\left(\frac{Q_1(t)}{\pi\hbar}\right)\exp\left(-\frac{Q_2(t)}{\pi\hbar}\right), \tag{6}$$

with

$$Q_1(t) = \int_0^\infty d\omega \frac{J(\omega)}{\omega^2} \sin \omega t, \tag{7}$$

and

$$Q_2(t) = \int_0^\infty d\omega \frac{J(\omega)(1 - \cos \omega t)}{\omega^2} \coth\left(\frac{\hbar\omega}{2k_B T}\right). \tag{8}$$

In the high temperature limit, where equipartition holds for all modes coupled to the ET, the SBM reproduces the well-known Marcus expression for the electron transfer rates,

$$k(\epsilon, T) = \frac{2\pi}{\hbar} V^2 \frac{1}{\sqrt{4\pi\lambda k_B T}} \exp\left[-\frac{(\epsilon - \lambda)^2}{4\lambda k_B T}\right], \tag{9}$$

where the energy gap, ϵ, and the reorganization energy, λ, are defined so they both have positive values for an exothermic reaction, k_B is the Boltzmann constant, T is the absolute temperature, and λ is related to $J(\omega)$ by (Xu and Schulten, 1994)

$$\lambda = \frac{1}{\pi}\int_0^\infty \frac{J(\omega)}{\omega} d\omega. \tag{10}$$

At low temperatures the classical (Marcus) picture fails completely, and the specific shape of the spectrum $J(\omega)$ governs the temperature dependence of the ET rate coefficient. Physically, this is due to the zero point motion of the vibrational modes coupled to the ET, which is ignored in Eq. 9. Other approximations to the SBM are possible (Levich and Dogonadze, 1959; Jortner, 1976; Schulten and Tesch, 1991), but they either place restrictions on the choice of $J(\omega)$ or are not valid for all temperatures. (The common approximation of discrete modes coupled to ET corresponds to choosing $J(\omega)$ to be a sum of δ functions.) Thus we prefer the more complex expression, Eq. 6.

The exact expression for the electronic matrix element, V, depends on the model used (Hopfield, 1974; Beratan et al., 1985), but the WKB (semiclassical) tunneling approximation (Sakurai, 1985),

$$V \propto \exp(-\sqrt{2m_e|\Delta E|}d/\hbar), \tag{11}$$

is detailed enough for our purposes. Here, m_e is the mass of the electron, ΔE is an average energy deficit of $P^+Q_A^-$ and PQ_A below the multitude of bridging electronic states that

mediate the electron transfer, and d is the distance between P and Q_A. From ET rate measurements on a variety of different systems, the approximate empirical relation

$$k \propto |V|^2 \propto \exp(-\beta d), \tag{12}$$

with $\beta = 1.4$ Å^{-1}, was obtained for α-helical proteins (Moser et al., 1992), yielding a value of 1.8 eV for ΔE in Eq. 11. Consequently, a factor 2 change in V (a factor 4 change in k) will result from a change in d of 1.0 Å, or a change in ΔE of 140 meV, assuming a P–Q_A distance of 25 Å.

Simplifying assumptions

To construct a viable model of electron transfer rates, we make two simplifying assumptions: 1) The logarithm of the electronic coupling V varies only as an explicit linear function of ϵ, independent of temperature and conformation; and 2), the spectral density $J(\omega)$ is a smooth function, independent of temperature and conformation. Although we rationalize these assumptions below with physical arguments, their ultimate justification lies in the ability of this model to accurately fit the ET kinetics with a minimal number of parameters and self-consistently explain a variety of phenomena associated with relaxation and disorder in reaction center proteins.

In our SBM calculation, ϵ (Eq. 6) is the difference in energy between $P^+Q_A^-$ and PQ_A, whereas ΔE (Eq. 11) is the average deficit of these two states below the multitude of bridging electronic states. Because the changes in ϵ are small compared to the magnitude of ΔE, we expect a coupling between log V and ϵ of the form

$$\log V = \log V_0 + \gamma(\epsilon - \epsilon_0), \tag{13}$$

where V_0 is the value of V at the (arbitrarily chosen) energy gap ϵ_0. The coefficient γ will be positive if the energy of $P^+Q_A^-$ changes more than that of PQ_A, and will be negative if PQ_A changes more than $P^+Q_A^-$. If the relaxations of $P^+Q_A^-$ and PQ_A are equal and opposite, γ equals zero. Another mechanism that leads to a change in V after ET is a change in the donor-acceptor separation. Because d also appears in the exponent of Eq. 11, a logarithmic relation like Eq. 13 will be expected in this case as well.

Equation 13 allows us to account for conformational changes affecting both ϵ and V, but without distinguishing the relaxation of two independent distributions. Both ϵ and V are distributed and treated equivalently in the analysis; a distribution in V is a distribution in ϵ, and a relaxation of V is a relaxation of ϵ. Our choice to discuss the heterogeneity in terms of ϵ rather than V is due to its additional connection to the free energy of the protein as a whole.

As temperature decreases, thermal contraction is likely to increase V because of the decrease in d of Eq. 12. If we take the data on myoglobin as typical for thermal contraction in proteins, we expect a decrease in linear dimensions of 1.4% upon cooling from room temperature to 80 K (Frauenfelder et al., 1987). With a donor-acceptor separation d of 25 Å, Eq. 12 predicts an increase in the ET rate k of ~40%, compared with the observed increase by 670%. This estimate suggests that temperature-dependent changes in V can be neglected. If the bridging states are antibonding orbitals, which move upward in energy as the bonded atoms move together, it is possible that the effect on V of a decrease in d is partially compensated by an increase in $|\Delta E|$ (see Eq. 11), making the temperature-dependent changes in V even smaller.

In our SBM calculation, the correlation time of energy gap fluctuations is on the order of $\hbar/0.5$ eV ≈ 8 fs, which is much shorter than even the vibrational periods of the energy-accepting modes. Consequently, $J(\omega)$ depends only on the coupling of vibrational states to ET, which is governed by typical bond strengths, atomic masses, and the magnitude of partial charges. These properties are not expected to change appreciably with temperature or conformation. Thus we use a single $J(\omega)$ for all temperatures and conformations to calculate the electron transfer rate. We assume a smooth $J(\omega)$ because it simplifies the calculations substantially. A rough $J(\omega)$ will lead to a rough $k(\epsilon)$ at low temperatures. Consequently, interpolation of rates in both ϵ and temperature becomes unreliable, and Eq. 6 would need to be evaluated at many more values of ϵ and T.

Our model, then, is based on Eq. 5, with FC given by Eq. 6 and V given by Eq. 13. The heterogeneity in the protein ensemble is modeled entirely by distributions, $g(\epsilon)$, of the energy gap between $P^+Q_A^-$ and PQ_A. The relation

$$g(\epsilon)\mathrm{d}\epsilon = f(k)\, d\log k \tag{14}$$

enables us to convert the energy distributions into rate distributions by using the calculated $k(\epsilon)$ at the appropriate temperature.

With $f(k)$ calculated from the model, the observed ET kinetics, $N(t)$, can be obtained with Eq. 2. Alternatively, we can express the observed electron transfer kinetics, $N(t)$, directly in terms of an energy distribution, $g(\epsilon)$:

$$N(t) = \int_{-\infty}^{\infty} g(\epsilon) \exp(-k(\epsilon)t)\, \mathrm{d}\epsilon. \tag{15}$$

This approach allows quantitative comparison of the experimental data with the model on the basis of one specific measure of protein conformation, the energy gap ϵ.

Parameter determination

Both conformational changes (changes that affect $g(\epsilon)$) and the inherent temperature dependence of the ET rate ($k(\epsilon, T)$ in Fig. 3 *a*) are responsible for the temperature dependence of k_{ET} in Fig. 2. By cooling under illumination from T_L = 110 K and observing that the changes annealed completely by 40 K, we demonstrated that, between 40 and 110 K, the second effect dominates on the warming time scale. Therefore, the low temperature kinetics in Fig. 1 *a* can be used to

determine the three temperature-independent quantities in our ET model, $J(\omega)$, V_0, and γ.

The shape of $J(\omega)$ is determined from the temperature dependence of k_{ET}, which becomes progressively weaker as the temperature is lowered, because the vibrational motions reach their zero point energies ($k_BT \approx \hbar\omega$), and nuclear motions no longer depend on temperature. The behavior between 140 and 5 K (Fig. 2 *a*) requires $J(\omega)$ to have substantial contributions from modes broadly distributed below 100 cm^{-1}. We chose to parameterize the spectral density with a continuum of such low-frequency modes, plus broad distributions at higher frequencies, to reproduce the temperature dependence of the ET rates in Fig. 2 *a* with minimal conformational changes (changes in $g(\epsilon)$) between 40 and 110 K on the time scale of sample warming. (Inclusion of some high-frequency modes ($\omega > 200$ cm^{-1}) can be accommodated (accounting for ~20% of the reorganization energy), subject to the constraints given in the caption to Table 1. They will, however, decrease the ability of our model to reproduce the absence of conformational change on the warming time scales between 50 and 120 K.) $J(\omega)$ is plotted in Fig. 3 *a*, and the complete parameterization is given in Table 1 and its caption. Molecular dynamics simulations support a picture in which a continuum of modes with energies $\hbar\omega < 100$ cm^{-1} accepts most of the energy during the electron transfer reaction (Warshel et al., 1989; Schulten and Tesch, 1991; Treutlein et al., 1992). As the temperature is raised, the specific shape of $J(\omega)$ matters less and less; in the high temperature limit, $k_BT > \hbar\omega$, Eq. 9 applies, and the shape of $J(\omega)$ is irrelevant.

Any value of the reorganization energy, λ, can be obtained by scaling $J(\omega)$ by an appropriate factor (see Eq. 10). To obtain the correct normalization, we exploit a peculiarity of activationless ET. Fig. 3 *a* shows that the $k(\epsilon)$ curves for different temperatures cross one another, and Fig. 3 *b* shows the temperature dependence of $f(k)$ produced by a temperature-independent $g(\epsilon)$ distribution. For RC molecules with $\epsilon > 520$ meV, the ET rate k decreases with increasing temperature, whereas for RCs with $\epsilon < 520$ meV, k increases with temperature. Examination of Fig. 1 *c* shows that the isokinetic point lies at $\log k = 1.1$. Choosing $\lambda = 667$ meV places the isokinetic point at 520 meV and the light-adapted conformation close to $\epsilon = 0.5$ eV, in agreement with the value known from redox titration (Lin et al., 1994) or delayed fluorescence (Arata and Parson, 1981). We place the light-adapted distribution here because it is the light-adapted conformation from which recombination occurs at room temperature.

Once we have decided on the spectral density shown in Fig. 3 *a* (*inset*), the SBM predicts the ratio of the fastest possible rate to the rate at the isokinetic point to be ~2, for constant V. Introducing the interdependence of V and ϵ (Eq. 13), with γ equal to 0.0014 decades/meV, reproduces the observed value of 7 (see Fig. 1 *c*). Finally, V_0 is simply a multiplicative factor that scales *FC* to the actual ET rate in [s^{-1}]. Values of all model parameters are compiled in Table 1, and the resulting $k(\epsilon, T)$ curves are shown in Fig. 3 *a*.

Qualitative support of our ET model is provided by the ability of a Gaussian ϵ distribution to reproduce the distinctive shape of the rate distributions shown in Fig. 1 *c*. This can be quantified by comparing the reduced χ^2 for several different fits of the normalized ET kinetics at 5 K for the sample cooled in the dark. The time-dependent errors in the data were $\sim 10^{-3}$ in transmittance space, as determined from the shot-to-shot variation in the kinetics. A single-exponential fit (one parameter) yields $\chi^2 = 175$, a Gaussian $f(k)$ distribution (two parameters) yields $\chi^2 = 2.2$, a Gaussian $g(\epsilon)$ distribution (two parameters plus model) yields $\chi^2 = 0.78$, and a two-exponential fit (three parameters) yields $\chi^2 = 0.62$. The ET model not only provides physical meaning, but also eliminates one arbitrary parameter from the fitting procedure.

At 5 K, the ET kinetics of light-cooled RCs are dispersed over three decades and cannot be adequately fitted by a single Gaussian $g(\epsilon)$ distribution (or two exponentials), so we used a two-Gaussian $g(\epsilon)$. The second Gaussian was used only below 175 K for the sample with $T_L = 280$ K. Because the two Gaussians overlap strongly, the combined distribution, shown in Fig. 3 *a*, is unimodal, and we also characterize it with an average energy $\langle\epsilon\rangle$ and standard deviation σ_ϵ, using Eqs. 3 and 4. In Fig. 4, the data in Fig. 2 are plotted in terms of $\langle\epsilon\rangle$ and σ_ϵ as a function of temperature; the parameters for data taken at 5 K are given in Table 2.

We can evaluate the success of our ET model by checking whether it reproduces the observation that no relaxations occur between 40 and 110 K on the time scale of warming. We see that it does, because both light- and dark-adapted samples show the same change in $\langle\epsilon\rangle$ with temperature, which results from 100-ms relaxations of the protein occurring in both the light- and dark-cooled samples. Furthermore, we see that the light-cooled conformation for $T_L =$

TABLE 1 Temperature-independent parameters of the ET model

V_0	γ	λ	S_S	S_{100}	S_{150}	S_{200}	S_{250}
1.81×10^{-4} cm^{-1}	0.00141 decades/meV	667 meV	19	6.4	5.7	3.2	4.6

V_0 at $\epsilon = 485$ meV and γ, which determine the electronic wavefunction overlap, are defined in Eq. 13. The coupling strengths S determine $J(\omega)$ by the equation $J(\omega)/\omega = S_S/(1 + (\omega/\omega_S)^2) + \Sigma_{i=1}^{4} S_{\omega_i} G(\omega_i, \sigma_i)$, where $\hbar\omega_S = 60$ cm^{-1} and S_{ω_i} is the area of a Gaussian distribution of modes (G), centered at an energy $\hbar\omega_i$ with standard deviation $\sigma_i \approx 0.15\ \omega_i$. $J(\omega)$ was truncated at 0 and 400 cm^{-1} (see *inset* of Fig. 3 *a*). The reorganization energy λ is defined in Eq. 10. We note that $J(\omega)$ is not uniquely determined; any broad distribution with similar values of λ and $\int_0^\infty J(\omega)d\omega$, which determines the width of $k(\epsilon)$ at low temperatures, would yield similar results.

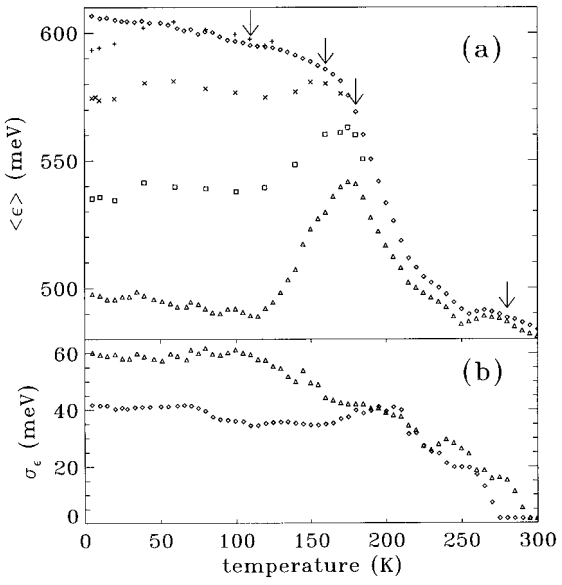

FIGURE 4 (*a*) Peak positions and (*b*) widths of the $g(\epsilon)$ distributions resulting from fits to electron transfer kinetics, using the model calculation shown in Fig. 3. The symbols correspond to those in Fig. 2.

TABLE 2 Low temperature (5 K) distributions

	$\log(k_{ET}/s^{-1})$	σ_k (decades)	$\langle\epsilon\rangle$ (meV)	σ_ϵ (meV)
Dark	1.60	0.20	607	42
T_L = 110 K	1.54	0.21	593	41
T_L = 160 K	1.42	0.29	574	47
T_L = 180 K	1.15	0.37	534	47
T_L = 280 K	0.80	0.62	499	60

Values are average and standard deviation of distributions describing $P^+Q_A^- \rightarrow PQ_A$ ET kinetics at 5 K after cooling RC in the dark or under illumination from various temperatures T_L. Rate distributions, $f(k)$, are defined by Eq. 2, and energy distributions, $g(\epsilon)$, are defined by Eq. 15. They are related to each other (Eq. 14) by the $k(\epsilon, 5\text{ K})$ curve shown in Fig. 3 *a*. Both $f(k)$ and $g(\epsilon)$ distributions are plotted in Fig. 3 for RC cooled in dark and light with T_L = 280 K. All $g(\epsilon)$ are Gaussian, except for T_L = 280 K, which is the sum of two Gaussians, with $\langle\epsilon\rangle$ = 515 and 440 meV, σ_ϵ = 35 and 46 meV, and areas of 0.78 and 0.22, respectively.

280 K has approximately the same $\langle\epsilon\rangle$ at 5 K as is observed at 300 K, as it must if we are trapping the charge-separated conformation.

PROTEIN CONFORMATION

Structural heterogeneity

The electron transfer model presented in the previous section enables us to characterize the nonexponential ET kinetics of a heterogeneous sample of RC proteins with a distribution $g(\epsilon)$ of the energy gap between $P^+Q_A^-$ and PQ_A. A weighted nonlinear least-squares routine provides the position and width of a Gaussian $g(\epsilon)$ such as the one shown in Fig. 3 *a* for 5 K, which best reproduces the ET kinetics (*lines* in Fig. 1, *a* and *b*). Parameters of the distributions at 5 K are given in Table 2. Based on the ET model, ϵ distributions were determined for all temperatures explored, and the averages, $\langle\epsilon\rangle$, and standard deviations, σ_ϵ, are plotted as a function of temperature in Fig. 4. These data provide the time and temperature dependence of protein motions in terms of ϵ.

The energy gap ϵ is the difference between the energy of the protein/solvent system in the two electronic states involved in ET, $P^+Q_A^-$ and PQ_A. The value of ϵ depends on the conformation of the protein, which we represent by a conformational coordinate in Fig. 5. The average structure in the PQ_A state, around which the protein tends to fluctuate, is represented by a minimum in the free energy surface (*solid line*), and the heterogeneity in this state is indicated by the Gaussian centered over this minimum (*dotted line*). The same description applies to the charge-separated state, $P^+Q_A^-$ (*dashed line*), except that the fluctuations will be about a different average structure. The relative placement of the surfaces is determined by the low temperature ϵ distributions in Fig. 3 *a*, which correspond to the Gaussians along the conformational coordinate in Fig. 5. When the sample is cooled in the dark, the protein molecules are frozen in the distribution determined by the PQ_A energy surface, with $\langle\epsilon_{dk}\rangle$ = 607 meV. When cooled under illumination from 280 K, the proteins are frozen in a distribution determined by the $P^+Q_A^-$ energy surface, with $\langle\epsilon_{lt}\rangle$ = 499 meV, as given in Table 2.

Structural adaptations will change ϵ; we expect these to include dielectric relaxations of protein and solvent, changes of protonation state, domain shifts, and rearrangement of cofactors in their pockets. It is apparent that $\langle\epsilon\rangle$ must decrease monotonically when the protein adapts to the $P^+Q_A^-$ state and must increase monotonically during adaptation to the PQ_A state. It is also necessary that every conformational change with an equilibrium affected by charge separation be reflected in a relaxation in $\langle\epsilon\rangle$.

At 5 K, the standard deviations of the energy distributions, σ_ϵ, of the proteins that were cooled under illumination from various temperatures are all similar (Table 2). This observation suggests that the proteins remain structurally intact when cooled under illumination. They simply visit

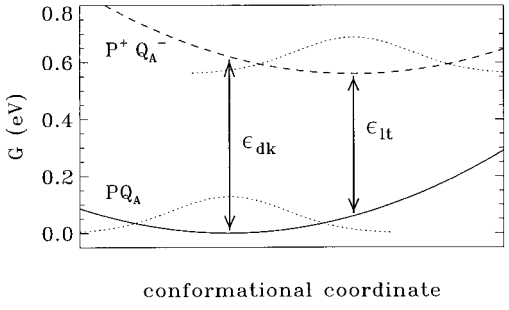

FIGURE 5 Schematic of the free energy surfaces that govern the protein conformation in the $P^+Q_A^-$ and PQ_A states. The energy gaps, ϵ, at the center of both the light- and dark-adapted distributions are indicated. The widths of the Gaussian distributions ($\cdots$) are determined by the $g(\epsilon)$ distributions in Fig. 3. Because the parabolic energy surfaces have the same shape, ϵ is linear in the conformational coordinate shown.

different sets of CSs that are energetically more favored when in the $P^+Q_A^-$ state. The Gaussian shape of the distribution that is obtained upon cooling in the dark is consistent with many small and uncorrelated structural differences between CSs. In the light-adapted state, an additional low energy tail and loss of signal amplitude (see caption to Fig. 1) indicate more significant structural changes upon charge separation in some of the proteins, for instance, those due to displacement of the charged Q_A^-.

Protein relaxation

At low temperature (5 K), in a sample that has been cooled in the dark, charge recombination occurs in a nonrelaxed conformation, with $\langle\epsilon\rangle = 607$ meV. Upon warming to 160 K, $\langle\epsilon\rangle$ decreases by 20 meV (Fig. 4 *a*), whereas the width of the distribution, σ_ϵ, stays fairly constant (Fig. 4 *b*). By 220 K, $\langle\epsilon\rangle$ has decreased by 105 meV, and a transient increase in σ_ϵ is seen. Both observations indicate the onset and development of the capacity of the protein to relax toward the light-adapted ($P^+Q_A^-$) state on the time scale of the charge recombination, ~100 ms.

After the sample is cooled under illumination, charge recombination occurs in an ensemble with $\langle\epsilon\rangle = 499$ meV and $\sigma_\epsilon = 60$ meV (see Table 2). Between 120 and 250 K, both the average value and the standard deviation of the energy distribution steadily approach the values observed for the sample cooled in the dark. The RC proteins that were frozen in the light-adapted conformation are increasingly able to return to the dark-adapted conformation, and we observe relaxation toward the dark-adapted (PQ_A) state on the time scale of sample warming, which is $\sim 10^4$ s (vida infra).

On warming of the sample cooled in light from 280 K, $\langle\epsilon\rangle$ reaches a maximum value at 175 K, which is only two-thirds that of the dark-adapted value. At this temperature, the dark-adapted value of $\langle\epsilon\rangle$ has decreased by 25% from its value at 5 K. Thus comparison of the light- and dark-adapted curves shows that at 175 K, 25% of the conformational energy is dissipated in less than 100 ms, whereas another 25% does not relax, even in 10^4 s.

Our model does not invoke or allow for temperature dependence of the protein structure that affects ET model parameters other than those determining $g(\epsilon)$. The validity of this approach is supported by the observation that the energy gap at room temperature is almost identical to the energy gap observed below 110 K when the sample is cooled under illumination (Fig. 4 *a*). This behavior is expected if 1) the sample recombines at room temperature from the same conformation (adapted to the charge-separated state) that is trapped by cooling under illumination, and 2) temperature-dependent changes of the protein, such as thermal expansion, result in negligible changes in the SBM parameters, as discussed above.

Fluctuational averaging

Below 160 K, σ_ϵ of the sample cooled in the dark (Fig. 4 *b*, *diamonds*) is constant because conformational changes are much slower than k_{ET}; the protein is effectively frozen in the PQ_A conformation on the time scale of ET. The increase in σ_ϵ at 195 K is due to the concurrence of relaxation with ET, $\kappa \approx k_{ET}$, giving a time-dependent (decreasing) rate coefficient. At temperatures above 220 K, a narrowing of the apparent ϵ distribution is observed. This behavior does not indicate that the actual distribution narrows with increasing temperature (it should widen), but that each molecule fluctuates among CSs with different energy gaps during the time that the charge-separated state persists. In the presence of fluctuations, the ET rate coefficient is given by an average over the CSs visited. With increasing temperature, the fraction of CSs that interconvert rapidly on the time scale of ET, or fluctuationally average, increases until all RCs fluctuate among CSs with values of ϵ representative of the entire $g(\epsilon)$ distribution, resulting in exponential recombination above ~260 K.

If we denote the distribution of energy gaps that each protein is able to visit during the lifetime of the charge-separated state by $g_{fa}(\epsilon)$, the averaged rate, $\langle k\rangle$, is given by

$$\langle k\rangle = \int_{-\infty}^{\infty} k(\epsilon) g_{fa}(\epsilon) d\epsilon. \tag{16}$$

Note that $\langle k\rangle$ differs from the ET rate at the average value of $g_{fa}(\epsilon)$. Consequently, the peak position (first moment) of the apparent $g(\epsilon)$ distribution in Fig. 4 *a* does not reflect the average energy gap about which the protein is fluctuating, but overestimates this value, because higher values of ϵ result in higher ET rates and so count more in the average. The amount of this overestimation depends on the width of $g(\epsilon)$ and the average slope of k versus ϵ. If, for instance, we assume a Gaussian $g(\epsilon)$ centered at 477 meV, with a width of 100 meV, at 300 K, complete fluctuational averaging will result in an apparent $g(\epsilon)$ centered at 485 meV with a width of zero, as observed in the data (Fig. 4 *a*). This shift of 8 meV is approximately given by

$$\Delta\epsilon = \Delta k \left.\frac{d\epsilon}{dk}\right|_{\langle\epsilon\rangle}, \tag{17}$$

where Δk is the difference between the fluctuationally averaged rate, $\langle k\rangle$, and the rate at the average of the $g(\epsilon)$ distribution, $k(\langle\epsilon\rangle)$,

$$\Delta k = \int_{-\infty}^{\infty} g(\epsilon) k(\epsilon) d\epsilon - k(\langle\epsilon\rangle), \tag{18}$$

with $k(\langle\epsilon\rangle) = k(\int_{-\infty}^{\infty} \epsilon\, g(\epsilon) d\epsilon)$. In our case, the shift is small, because of the very small slope, $dk/d\epsilon$, characteristic of activationless ET, so we neglect it. The small shift also indicates that conformational fluctuations of the protein are not important in determining $J(\omega)$, in contrast to the so-

called solvent-controlled ET (Rips and Jortner, 1987; Onuchic, 1987).

Finally, we briefly address the small dip that appears in $\langle\epsilon\rangle$ versus T near 250 K (Fig. 4 *a*). Additional measurements (data not shown) indicate that, at this temperature, slow changes in the protein conformation occur that are not caused by the charge separation process or illumination, but depend only on the residence time of the sample at 250 K. Because the light-cooled sample in Fig. 4 *a* was warmed more slowly than the dark-cooled sample, it shows a larger dip, centered at a slightly lower temperature. With minimal waiting time, the dip disappears. This effect may be associated with aggregation of RC molecules or crystallization of solvent molecules at the protein surface.

ENERGY LANDSCAPE IN RCs

Motion along the conformational coordinate sketched in Fig. 5 is inhibited by free energy barriers. The wide range of temperatures at which conformations can be trapped demonstrates that the barriers between CSs vary greatly in size. The similar temperature dependence of ϵ for samples cooled under illumination from different temperatures (Fig. 4 *a*) shows that the conformational barriers encountered at low temperatures do not depend in a systematic way on the value of the conformational coordinate. The small barriers are similar within each different region of conformational space separated by high barriers.

We have studied the dynamics of interconversion between CSs with two different protocols. 1) After the protein was trapped completely in the light-adapted conformation, the sample was slowly warmed, and ET kinetics were measured with a laser flash at 5-K intervals. This protocol was carried out at two different warming rates, 1.3 and 13 mK/s. Progressive changes in the ET kinetics reflect relaxation toward the dark-adapted state. 2) After the sample was cooled in the dark, the nonexponential ET kinetics reveal the ability of the protein to relax from the dark-adapted to the light-adapted conformation during the time that charge separation persists, ~100 ms. Thus we were able to study protein dynamics on three different time scales ranging over five orders of magnitude, which allowed us to analyze the energetics of relaxation. The use of an ET model to convert from rate to energy is critical for the comparison of relaxations in different directions and at different temperatures.

Relaxation functions

To quantify the extent of relaxation, we need a measure of the progress along the conformational coordinate in Fig. 5. For the sample cooled in the dark, $\langle\epsilon\rangle$ itself is such a measure, and we simply scale it from zero to one to obtain the relaxation function,

$$\Phi_{dk}(T) = \frac{\langle\epsilon_{dk}(T)\rangle - \langle\epsilon_{dk}(300K)\rangle}{\langle\epsilon_{dk}(5K)\rangle - \langle\epsilon_{dk}(300K)\rangle}, \quad (19)$$

where the values for ϵ are taken from Fig. 4 *a*. Φ_{dk} measures relaxation along the $P^+Q_A^-$ surface in Fig. 5 on the time scale of ET (100 ms). $\Phi_{dk} = 1$ represents the most unrelaxed protein detectable on the time scale of ET, with $\langle\epsilon\rangle$ = 607 meV, and $\Phi_{dk} = 0$ represents the completely relaxed protein, with $\langle\epsilon\rangle$ = 485 meV.

To measure relaxation of the sample cooled under illumination toward the dark-adapted conformation on the time scale of sample warming, 10^3 or 10^4 s (to the left along the PQ_A surface in Fig. 5), we define a similar relaxation function, Φ_{lt}, from the difference $\epsilon_{dk} - \epsilon_{lt}$, normalized by the same total energy span of relaxation as for Φ_{dk} above,

$$\Phi_{lt}(T) = \frac{\langle\epsilon_{dk}(T)\rangle - \langle\epsilon_{lt}(T)\rangle}{\langle\epsilon_{dk}(5K)\rangle - \langle\epsilon_{dk}(300K)\rangle}, \quad (20)$$

although slight differences in the light-cooled samples required us to scale Φ_{lt} of the sample warmed at 13 mK/s by a factor of 1.07. (In a temperature ramp experiment, the time scale probed depends on both the warming rate and the activation energy of the motion involved. From measurements at two different warming rates, it is possible to determine the time scale, as we do in the following sections.)

The three relaxation functions obtained from the data are plotted in Fig. 6 *a* as a function of temperature. As expected, relaxations occur at lower temperatures when the observation time scale is longer. By comparing the two Φ_{lt} functions for tenfold different warming rates (1.3 mK/s and 13 mK/s), we see that, between 120 and 180 K, these relaxation processes speed up by an order of magnitude in rate when the temperature is raised by ~7 K. Thus the difference of 35 K between Φ_{lt} for slow warming and Φ_{dk} is consistent with the 10^5 ratio of time scales probed by the two methods.

Barriers to relaxation

To relate the three relaxation functions, Φ, to one another, we need a model that predicts the temperature dependence of the rates of conformational transitions, $\kappa(T)$. By far the most widely used relation is the Arrhenius Law,

$$\kappa(T) = A_A \frac{T}{T_0} \exp(-E_A/k_B T), \quad (21)$$

where A_A is a preexponential factor, E_A is an enthalpy barrier to the transition, T is the absolute temperature, T_0 is a reference temperature (which we take to be 100 K), and k_B is the Boltzmann constant. This equation can be understood in terms of a thermally activated transition over a one-dimensional barrier of height E_A.

In systems in which cooperative transitions are involved, such as proteins and viscous solvents, Ferry's Law (Ferry et al., 1953; Frauenfelder and Wolynes, 1994),

$$\kappa(T) = A_F \exp - (E_F/k_B T)^2, \quad (22)$$

often provides a better description of the rate coefficients. Note that A_F and E_F have an interpretation different from

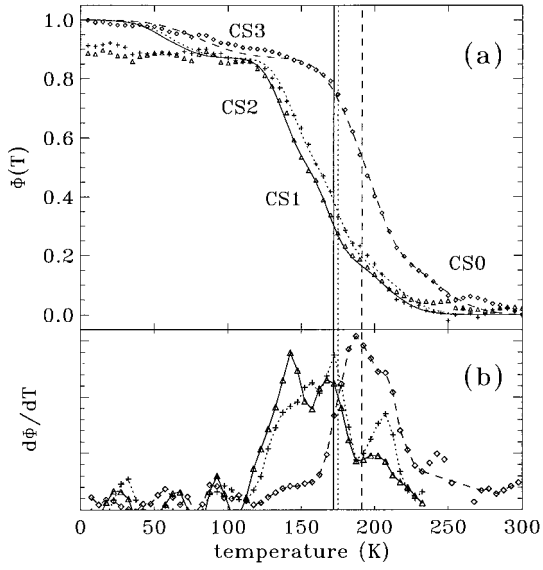

FIGURE 6 (*a*) Relaxation functions, $\Phi_{lt}(T)$, calculated with Eq. 20 from the data in Fig. 4, as a function of temperature for warming rates of 1.3 (△) and 13 mK/s (+), and $\Phi_{dk}(T)$ (◇), calculated with Eq. 19 and the data in Fig. 4. The fit to $\Phi_{lt}(T)$ for warming rates of 1.3 (—) and 13 mK/s (····) was calculated with Eq. 23, and the fit to $\Phi_{dk}(T)$ (– – –), calculated with Eq. 24, used the Arrhenius Law (Eq. 21 and the parameters in Table 3). Φ_{lt} (····) for the sample annealed at 1.3 mK/s was scaled by a factor of 1.07. Each tier of CS is indicated. Vertical lines indicate the temperature at which solvent relaxations occur in 10^4 s (—), 10^3 s (····), and 100 ms (– – –). (*b*) Derivatives, $d\Phi/dT$, of smoothed Φ presented in *a*. Symbols correspond to those in *a*. The peaks visible in $d\Phi_{lt}/dT$ of the sample warmed at 1.3 mK/s at 140, 165, and 205 K correspond to CS2, CS1, and CS0, respectively. CS3 is not clearly visible. A peak is seen at the solvent relaxation temperature in the $d\Phi/dT$ for each time scale. The straight dashed line in $d\Phi_{dk}/dT$ from 230 to 270 K and omission of data above 230 K in $d\Phi_{lt}/dT$ are to prevent the process at 250 K, described in text, from being misinterpreted as part of the relaxation functions.

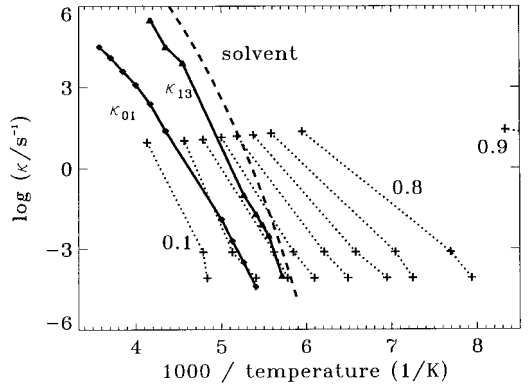

FIGURE 7 Arrhenius plot constructed from the relaxation curves in Fig. 6. The temperatures at which Φ_{lt} reaches values of 0.9, 0.8, and so on, are plotted at 10^{-3} and 10^{-4} s^{-1} for the fast and slow warming rates, respectively. The temperature at which Φ_{dk} reaches 0.9, 0.8, and so on, is plotted at k_{ET}. Solid lines labeled κ_{01} and κ_{13}: rates of exchange between taxonomic substates in carbonmonoxy myoglobin (Johnson et al., 1996); dashed line: temperature dependence of the peak rate of the dielectric loss of the solvent used in this study (3/1 glycerol/water, v/v), taken from Huck et al. (1988).

that of the analogous parameters in Eq. 21. Our range of rate coefficients is still too small to allow us to distinguish between these two relations. But, because they differ in their extrapolation to high temperatures, we present fits and extrapolations, using both relations.

It is possible to extract information about barriers and preexponentials from the relaxation functions that is independent of the particular parameterization of the data. We need only assume that the various relaxation events in RCs occur in the same sequence for all three relaxation functions in Fig. 6 *a*. This means that the crossing points of horizontal lines with the relaxation functions give the temperature at which a particular motion happens on each of the three different time scales (τ = 100 ms, 10^3 s, and 10^4 s) examined here. We then invert the time scales to obtain rate coefficients for conformational change, $\kappa = \tau^{-1}$. In Fig. 7, these rates are plotted against the inverse temperature in an Arrhenius plot (log κ versus $1/T$) for every 10th percentile of the relaxation function. The different slopes indicate that the activation energies differ widely. For the motions happening after 90% of the relaxation is complete (at $\Phi = 0.1$), barrier energies of 110 kJ/mol are obtained, in contrast to 70 kJ/mol at the level of $\Phi = 0.8$.

A more sophisticated analysis can be carried out by simultaneously fitting a set of preexponentials and energy barriers to all three relaxation functions in Fig. 6 *a*. To achieve a quantitative description, it was necessary to assume four Gaussian energy distributions, $g(E)$, each with a distinct preexponential factor A and a full width at half-maximum, Γ. This implies that the barriers between the conformational substates are arranged in four classes or tiers, each of which has a characteristic range of energies. In Fig. 6 *a*, the separation into tiers shows up as structure on the relaxation functions. This can be seen more easily in the first derivative, $d\Phi/dT$, plotted in Fig. 6 *b*, where each tier gives rise to a local maximum on the curve. We refer to the four tiers as CS0, CS1, CS2, and CS3, in order of decreasing barriers, following nomenclature introduced in studies of heme protein dynamics (Frauenfelder et al., 1991; Nienhaus and Young, 1996).

The kink seen at $\Phi = 0.2$ in Fig. 6 *a* in all three relaxation functions identifies the highest tier, CS0, for the slowest relaxations. On the 10^4 s time scale, its temperature range is 180–240 K. The relaxation between $\Phi = 0.85$ and 0.2 appears as a single, broad process in Φ_{dk}, but on the longer time scales, seen in Φ_{lt}, this part of the relaxation is dispersed into two processes, CS1 and CS2, of approximately equal amplitude. This distinction is clearly seen in the $d\Phi/dT$ data in Fig. 6 *b* on the time scale of 10^4 s, where tier 1 relaxations can be observed between 160 and 180 K, whereas the relaxations in CS2 occur between 130 and 160 K. Relaxations in the tier with the smallest barriers, CS3, appear in the range of $1 < \Phi < 0.85$ at temperatures below 100 K in Φ_{dk}. However, because we were unable to cryogenically trap CS3 completely, it is not clearly evident in Φ_{lt} for T_L = 280 K. Thus we cannot determine both preexponential and a barrier distribution for this tier.

Because Φ_{lt} and Φ_{dk} were measured in different ways, different formulas relate preexponentials A and barrier distributions $g(E)$ to Φ_{lt} and Φ_{dk}. If the sample is warmed at a constant rate β, Φ_{lt} is given by

$$\Phi_{lt}(T, \beta) = \sum_{i=0}^{3} \int_0^{\infty} g_i(E) \exp\left(- \int_{5K/\beta}^{T/\beta} \kappa(E, A_i, \beta t) dt \right) dE, \quad (23)$$

where the sum extends over the different tiers of CSs, $g_i(E)$ is the energy distribution characterizing conformational barriers in the ith tier, and $\kappa(E, A_i, T)$ is the relaxation rate coefficient, which can be given by either Ferry's Law or the Arrhenius Law. The exponent contains an integral to account for the variation of κ with time (because of the changing temperature), instead of the commonly encountered expression with a constant κt. Calculation of Φ_{dk} is simpler; the energy barriers are given by

$$\Phi_{dk}(T, \tau_{ET}) = \sum_{i=0}^{3} \int_0^{\infty} g_i(E) \exp(-\kappa(E, A_i, T)\tau_{ET}) dE, \quad (24)$$

where τ_{ET} is the inverse of the average ET rate k_{ET}, given in Fig. 2 *a*. This equation is greatly simplified because the extent of relaxation during the nonexponential recombination is small compared to the total relaxation. The fits are shown as lines in Fig. 6 *a*, and the parameters describing the barrier distributions are compiled in Table 3.

Characteristics of the energy landscape

The simultaneous fit of relaxation functions from three different time scales showed that energy is dissipated during protein relaxation on at least four distinct tiers, each characterized by a preexponential, a distribution of energy barriers to relaxation, and either the Arrhenius Law (Eq. 21) or Ferry's Law (Eq. 22). This procedure yields a quantitative characterization of protein relaxations, allowing extrapolation and interpolation of the data for comparison with isothermal relaxation experiments, and aiding our understanding of the physical mechanism of relaxation.

The dielectric relaxations of the solvent (75% glycerol/25% water, v/v) have been measured by Huck et al. (1988). They show a temperature and frequency dependence typical of glass-forming liquids, including a large apparent Arrhenius activation energy and non-Arrhenius temperature dependence. Comparison of solvent dynamics and RC relaxations can be made with Figs. 6 and 7. Fig. 6 shows the temperature of solvent motions on each relevant time scale as a vertical line, revealing that CS1 on both slow time scales is correlated with the solvent glass transition. Examination of $d\Phi/dT$ in Fig. 6 *b* shows clear peaks in the regime of solvent relaxation. The coincidence of the solvent glass transition with the steep part of the relaxation function and physical intuition both suggest a coupling between RC dynamics and the solvent. The interplay between protein and solvent dynamics has been characterized in previous studies in myoglobin (Beece et al., 1980; Ansari et al., 1994).

Relaxations in RCs differ considerably from those of simple glass formers, with the principal difference being the division of RC relaxations into four widely separated broad tiers of approximately equal size. As the temperature is lowered, the different tiers of motions freeze out successively. In the following, as we compare the motions on successive tiers of CSs, we emphasize how different activation enthalpies and time scales of motions imply different physical motions involved in each tier. Note that our relaxation functions weigh the tiers according to the energy dissipated.

The slowest 25% of the protein relaxation occurs in a group that we refer to as CS0. It is separated from the faster relaxation processes by a distinct kink in the relaxation function. The end of the relaxation is marked by the flatness of $\Phi(T)$, which is somewhat obscured, but clearly occurs by 250 K in $\Phi_{lt}(T)$. The large values of the parameters E_F and A_F, together with the observation that CS0 relaxation occurs more than 1000 times slower than solvent relaxations, imply that these slow relaxations are highly cooperative, needing sizable changes in protein conformation to occur. This ability to store conformational energy on time scales that are long compared to the solvent relaxation times may be a consequence of the complex structure of proteins.

A second set of cooperative motions, CS1, which appears on the same time scale as the solvent dielectric relaxations, accounts for 25% of the relaxation. However, examination of Fig. 6 shows that CS1 cannot be direct observation of

TABLE 3 Energy barriers to conformational change

Process	Amplitude	$\log(A_A/s^{-1})$	E_A (kJ/mol)	Γ_A (kJ/mol)	$\log(A_F/s^{-1})$	E_F (kJ/mol)	Γ_F (kJ/mol)
CS0	0.21	25	110	24	11.7	9.9	2.2
CS1	0.28	21	78	10	10.6	7.8	0.9
CS2	0.38	15	50	10	—	—	—
CS3	0.13	13	17	13	—	—	—

Values are amplitude, preexponential factors, mean, and full width at half-maximum of the four Gaussian distributions obtained from a global fit to the relaxation functions Φ_{dk} and Φ_{lt} shown in Fig. 6 *a*, using either the Arrhenius Law (Eq. 21) or Ferry's Law (Eq. 22). The preexponential for CS3 was fixed at 10^{13} s^{-1}. Ferry Law parameters for CS2 and CS3 are omitted because the Arrhenius parameters indicate that these motions are indeed appropriately modeled with the Arrhenius relation. Moreover, using a Ferry parameterization for CS2 and CS3 gives unreasonable results for the extrapolation to room temperature.

solvent relaxation for two reasons: 1) The change in rate with temperature of solvent relaxation, indicated by the vertical lines, is much greater than that of the protein relaxation, and 2) solvent relaxations occur in a much narrower temperature window than CS1 (Huck et al., 1988); they would be represented by a peak with a FWHM of 4 K in Fig. 6 *b*. Whether CS1 relaxations are motions directly coupled to the solvent or simply represent a glasslike process intrinsic to the protein that happens to have a glass transition temperature similar to that of the solvent can only be addressed by measuring the relaxation as a function of time and temperature in a variety of solvents.

On the 100-ms time scale, only one broad relaxation process is visible between CS0 and CS3 in Fig. 6 *a*. At lower temperatures or, equivalently, on longer time scales, this broad process splits into two parts, one of which, CS2, occurs in an immobile solvent. The Arrhenius preexponential of 10^{15} s^{-1} for CS2 is closer to that expected for a one-dimensional activated barrier crossing than that of either CS0 or CS1. Consequently, in this tier we expect transitions between the minima of independent double-well potentials in an otherwise immobile protein.

Motions between 40 and 110 K are absent in RCs on the 10^4 s time scale. This was useful for determination of the ET model parameters, $J(\omega)$ and $V(\epsilon)$, and indicates a gap in the distribution of barriers between CS2 and CS3.

The full amplitude of the relaxation in CS3 was only visible in Φ_{dk}, so it is not possible to uniquely determine both the preexponential and the size of the enthalpy barrier to transitions. There are two possible explanations for our apparent inability to cryogenically trap the light-adapted state in CS3 (Fig. 7): 1) The transition may occur by tunneling through a barrier at a temperature-independent rate of less than an hour below ~25 K, thus preventing cryogenic trapping on our very slow warming time scales. 2) The relation between V and ϵ (γ in Eq. 13) in CS3 may be different from that in the other tiers. Consequently, we arbitrarily assume an A_A of 10^{13} s^{-1}, which corresponds to a typical barrier crossing attempt frequency in transition state theory (Atkins, 1990). The time and temperature dependences of these relaxations correspond to those observed in temperature cycle hole burning experiments on horseradish peroxidase (Zollfrank et al., 1991), and we have not excluded the possibility that the relaxations involved occur in a photoactivated state (as opposed to the charge-separated state).

The motions in the four different tiers have been modeled with thermally activated processes because they gradually speed up with temperature. It is also possible for phase transitions (for example, thawing of surface water) to facilitate relaxations at one temperature on all time scales. This will lead to a peak in all three $d\Phi/dT$ at the same T. Indeed, such a feature appears in Fig. 6 *b* at 210 K. However, it is evident that the bulk of the relaxation is more appropriately described as activated barrier crossing.

Extrapolation to physiological conditions

Although study of relaxations at low temperatures provides the best separation of conformational changes into their component tiers, it is the behavior of proteins at higher temperatures that we ultimately wish to understand. The relaxation functions that we have presented quantify the extent to which static heterogeneity, relaxation, and fluctuational averaging are present in the protein ensemble. The barrier distributions described in Table 3 allow us to calculate isothermal relaxation functions as

$$\Phi(t, T) = \sum_{i=0}^{3} \int_0^\infty g_i(E)\exp(-\kappa(E, A_i, T)t)dE, \quad (25)$$

where the notation is the same as in Eq. 23. Calculated relaxation functions are plotted in Fig. 8 for several temperatures, and vertical lines indicate the three time scales at which $\Phi(T)$ was determined.

At 300 K, we see a smooth, featureless decay of $\Phi(t)$ from 10 ps to 1 ms. From this we learn, for example, that at 10 ns, ~40% of the relaxations are completed. For the majority of CSs, however, we need to consider a static distribution of protein conformations as well as time evolution of properties for the 10% of relaxations with $\kappa \approx 10$ ns. Because the width of the static distribution is similar to the total extent of relaxation (see Fig. 3 or 5), it is not appropriate to neglect either static heterogeneity or relaxation.

Fig. 8 indicates a practical difficulty encountered in measuring protein relaxations isothermally. Below 240 K, the slowest relaxations require more than 1 day to occur, but at 300 K, relaxations will have begun in a few picoseconds. Even an experiment that covers several orders of magnitude in time will capture only a fraction of the total relaxation. Unless a marker for relaxation is found that can be unambiguously compared at different temperatures, it will not be clear whether the same conformational change is being observed at each temperature. The temperature ramp experiments circumvent this problem by allowing each relaxation to be observed once, and only once, on each different time scale.

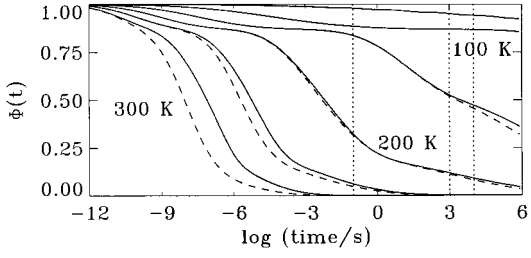

FIGURE 8 Isothermal relaxation functions calculated with the Ferry Law for CS0 and CS1 and the Arrhenius Law for CS2 and CS3 (—) or the Arrhenius Law for all tiers (– – –) and the parameters in Table 3, at 50, 100, 150, 200, 250, and 300 K. Vertical lines indicate the time scales at which $\Phi(T)$ was measured.

Our experiments were performed with RCs in a glycerol/water mixture (3/1, v/v). Measurements of rates of protein conformational motions derived from CO recombination kinetics in myoglobin and spectroscopic changes after flash photolysis in myoglobin both suggest that replacing the glycerol water mixture with water should speed up conformational changes by a factor of 6 at room temperature. The decreased viscosity is probably the most relevant change (Beece et al., 1980; Ansari et al., 1994).

DISCUSSION

A statistical treatment of the CSs in RC allows us to describe the ET event in terms of three protein properties—the distribution of CSs, $g(\epsilon)$; the temperature dependence of interconversion between CSs, $\Phi(t, T)$; and the parameters describing the fundamental ET process, $k(\epsilon, T)$. All of these can be determined by requiring a self-consistent description of our relaxation experiments. The relaxation function, $\Phi(t, T)$, can be described in terms of the energetics of interconversion among CSs on four distinct tiers, providing a basis for physical models of protein dynamics. Comparison to extensive studies of heme protein dynamics reveals similar relaxation properties and illustrates the variety of effects that these relaxations can have on protein function. In this section we relate our work to previous studies in each of these areas.

Electron transfer

A direct way to experimentally determine $k(\epsilon)$ is to apply an external electric field across the RC to change the energy of recombination, ϵ, and measure the flash-induced ET kinetics. With appropriate assumptions and control experiments, one can relate the shift in ϵ to the voltage applied across the sample. This has been done with RCs incorporated into a lipid bilayer with a small preferential orientation of functional RCs (Gopher et al., 1985). Within the experimentally accessible range, there was no detectable dependence of the rate on the applied field. However, the range of fields applied was limited to less than 3×10^5 V/cm. Using dried monolayers, also with perpendicular orientation, Popovic et al. (1986) were able to apply much larger fields and observed significant changes in the yield of charge separation. They also reported a ~10-fold change in the recombination rate, over a range of external field estimated to be 10^6 V/cm, but the disagreement with Gopher et al. (1985) and uncertainties in their exact experimental conditions make detailed comparison of their data to ours difficult.

Boxer and co-workers have carried out extensive studies on randomly oriented RCs in thin PVA (polyvinyl alcohol) films to which they could apply electric fields as high as 10^6 V/cm (Franzen et al., 1990). In the notation of our work, they broadened the existing distribution of energy gaps, $g(\epsilon)$, by applying an external electric field to the sample. Because the exact form and electric field dependence of the broadening is known, analysis of the rate distributions (or ET kinetics) allows determination of the dependence of the ET rate on energy, $k(\epsilon)$. Their experimentally determined $k(\epsilon)$ is in reasonable agreement with our findings, although somewhat broader. This may be due to the different treatment of the zero-field, dark-cooled kinetics, which they split into two independent processes obeying unrelated $k(\epsilon)$ relations, whereas we used a single distribution, subject to a single $k(\epsilon)$ curve. Additional uncertainty exists in that work because the value of the protein dielectric constant is uncertain (Steffen et al., 1994).

Another experimental method of determining $k(\epsilon)$ is to systematically vary the quinone redox potential by substitution of the native ubiquinone with other types of quinones (Gunner et al., 1986), or the special pair redox potential by amino acid substitution to change the number of hydrogen bonds to P (Lin et al., 1994). Gunner et al. (1986) first demonstrated that a substantial difference between ϵ and λ can exist in proteins that display activationless ET. They also showed that V varies by a factor of ~3 when substituting a wide variety of different types of quinone in the Q_A site, consistent with our observation that both ϵ and V depend on protein/cofactor conformation. The site-directed mutants of Lin et al. (1994) are a beautiful example of the use of proteins to observe the effects of specific modifications of a complex system at the atomic level. The slightly shallower slope they observed for $k(\epsilon)$ of the $P^+Q_A^- \rightarrow PQ_A$ ET may indicate a coupling of V and ϵ (γ in Eq. 13) upon modification of the electronic state of P that differs from the one observed here.

Three of the groups mentioned above extended their studies to low temperatures (Gunner et al., 1986; Franzen and Boxer, 1993; Ortega et al., 1996) and noted the peculiar temperature dependence of $k(\epsilon)$. They did not consider, however, the central importance of conformational change. Franzen and Boxer (1993) and Ortega et al. (1996) noted that the difference between λ and ϵ is larger at high temperature than at low, but because in the classical ET theory the rate coefficient depends on $\epsilon - \lambda$, they could not experimentally determine which quantity was temperature dependent. Note that Eqs. 9 and 10 imply that λ and ϵ affect the width of $k(\epsilon)$ differently, but the width of $k(\epsilon)$ also depends on $J(\omega)$, which is undetermined in earlier work by Franzen and Boxer (1993) and Ortega et al. (1996). Both groups chose to make λ temperature dependent, although Ortega et al. (1996) do point out that this would imply that ET is coupled primarily to vibrations of the solvent molecules. When their results are reinterpreted in terms of a changing ϵ and a fixed λ, the size of the shift (~120 meV) is in agreement with our results. Although we also measure only the difference, $\epsilon - \lambda$, we attribute the changes with time and temperature to ϵ for physical reasons, as explained in Quantitative Model of Electron Transfer.

In their figure 1, Ortega et al. (1996) have plotted the temperature dependence of the $P^+Q_A^- \rightarrow PQ_A$ for three mutants with energy gaps of 425, 500, and 580 meV. The data show an interesting behavior that is predicted by our

model of RC relaxation. Those mutants with large values of ϵ (600 meV) show a uniform temperature dependence of k from 10 to 300 K, whereas mutants with lower values of ϵ (500 meV) show temperature-independent k below 150 K, with a sharp decrease above 180 K. Examination of our relaxation function on the ET time scale in Fig. 6 *a* shows that ϵ is constant below 150 K and decreases rapidly with increasing temperature near 180 K. Thus the temperature dependence of the ET rate below 150 K will depend only on dk/dT, whereas near 180 K, it will depend on both dk/dT and $dk/d\epsilon$. Our calculated $k(\epsilon, T)$ curves in Fig. 3 reveal that, for $\epsilon \gtrsim 600$ meV, $|dk/dT|$ is large and $dk/d\epsilon$ is small, whereas for $\epsilon \approx 500$ meV, $|dk/dT|$ is small and $dk/d\epsilon$ is large. Thus the qualitatively different temperature dependence of the ET rate in this series of mutants is explained by our ET model. Furthermore, it makes specific quantitative predictions about the type of nonexponential kinetics expected in the various mutants; comparison with the mutant data should be illuminating.

Conformational substates in reaction centers

Dark-cooled ET kinetics can be, and often are, fitted with two exponential processes. This does not lead to identification of two physically meaningful states. Nonexponential kinetics of the $P^+Q_A^- \rightarrow PQ_A$ process, especially in RC samples cooled under illumination, led to the first introduction of distributions of CSs in RC (Kleinfeld et al., 1984). Their distribution of V to fit light-cooled and dark-cooled ET kinetics provided a parameterization of nonexponential kinetics that was mapped onto the physically meaningful properties of the average, width, and asymmetry of a distribution of distances. The analysis with Eq. 13, however, yielded somewhat large distance variations, and the model was not able to account for the temperature dependence of the reaction kinetics. We, by contrast, use a Gaussian ϵ distribution which is expected from a model with numerous CSs, with the disorder coming from a variety of contributions of comparable size.

CSs are also required to explain the multiexponential delayed fluorescence kinetics (Woodbury and Parson, 1986; Peloquin et al., 1994). The fluorescence arises from thermal repopulation of P^*H_A from the $P^+H_A^-$ state; adaptation of the protein to $P^+H_A^-$ creates a Boltzmann factor shifting the equilibrium further away from PH_A to $P^+H_A^-$ with time, leading to multiexponential fluorescence decay. The temperature dependence of the nanosecond decay component suggests that relaxation is occurring at high temperature. The fluorescence amplitude is smaller at 280 K than at 180 K, implying that the P^*H_A–$P^+H_A^-$ energy gap is larger at the higher temperature. This is most easily explained by assuming that protein relaxations can occur within a few nanoseconds after charge separation at 280 K, but not at 180 K. The relaxation of this energy gap, shown in Figure 6 of Woodbury and Parson (1986), can be compared directly with the relaxation of $P^+Q_A^-$–PQ_A (Fig. 6); it indeed occurs at a higher temperature than the relaxations we observed, as expected from the much shorter time scale involved (nanoseconds, compared to milliseconds or kiloseconds). We also find general agreement when comparing the 295 K relaxation data from figure 5 of Peloquin et al. (1994) with our extrapolated 300 K isothermal relaxation function in Fig. 8. Our data indicate that the relaxation should only have progressed about two-thirds of the way toward completion within a few nanoseconds, consistent with the observation that the energy gap of 1600 cm^{-1} observed at 10 ns by Peloquin et al. (1994) has increased to 2100 cm^{-1} on the microsecond time scale (Chidsey et al., 1985).

At lower temperature, we have observed nonexponential kinetics due to a static, temperature-independent distribution of energy gaps. Therefore, we also expect a static P^*H_A–$P^+H_A^-$ energy gap at low temperature. Unfortunately, such a distribution greatly complicates the analysis of delayed fluorescence (Ogrodnik et al., 1994), because the conversion from fluorescence intensity to energy then requires a weighted integral of the Boltzmann equilibrium factor over the entire energy gap distribution rather than its value at a single energy. However, there is not enough information in the data to determine the parameters of a distribution. This distinction will be of importance whenever the width of the distribution is larger than k_BT, as is expected at 20 K. Because the average fluorescence rate will be determined exclusively by that portion of the distribution having small values of the energy gap, it is extremely difficult to know where the energy gap is centered at low temperature. Because the fast-fluorescing RCs will soon be depleted, the energy gap will appear to increase with time. The exact time course of the apparent relaxation will depend on which portion of the distribution is near the zero energy gap (for example, the peak or the tail of a Gaussian), providing a possible explanation for the apparent dependence of relaxation properties on the presence or absence of single hydrogen bonds (Figure 5 *b* of Peloquin et al., 1994). Additional problems arise because the quantum yield of $P^+H_A^-$ formation is less than one. Should the quantum yield depend on the P^*H_A–$P^+H_A^-$ energy gap in a systematic fashion, comparison of experiments with different quantum yields will be complicated.

Although low temperature data, where static distributions are present (not to mention intermediate temperature data, where both relaxation and distributions are important), are difficult to interpret, we would like to emphasize the agreement of nanosecond relaxations of protein adaptation to $P^+H_A^-$ with those predicted from our measurements of adaptation to $P^+Q_A^-$ on the longer time scales.

Many groups have investigated the effects of protein CSs on the kinetics of primary charge separation (Kirmaier and Holten, 1990; Becker et al., 1991; Skourtis et al., 1992; Woodbury et al., 1994, 1995; Bixon et al., 1995). All have noted that an energy distribution of significant width (~100 meV) is consistent with experimental observations, although there is disagreement over such basic issues as whether the distributions of CSs are static or dynamic, and

whether ET is adiabatic or nonadiabatic. All groups agree on the complexity of the problem, and each points out different issues that make the data difficult to analyze and interpret. The determination of $\Phi(t, T)$ presented in this paper may aid in the understanding of this.

Relaxation and distribution of protein properties are related, and the connection between them was first explored by Rubin et al. (1994). They modeled the relaxation associated with the $P^+Q_A^- \rightarrow PQ_A$ ET kinetics with a distribution of CSs characteristic of PQ_A, which diffused to a distribution adapted to $P^+Q_A^-$, similar to our model. Simple diffusion, however, assumes a relaxation function $\Phi(t)$ that is exponential and not a function that extends over 10 orders of magnitude, such as our $\Phi(t)$ shown in Fig. 8. They recognized the problem and introduced a diffusion coefficient that changes with the position along the relaxation coordinate. Although this approach is an effective mathematical convenience, it is not a realistic physical model, because we have shown that the barriers are uniformly distributed along the conformational coordinate in Fig. 5.

Treatment of nonexponentially relaxing systems with numerous microscopic states is usually based on the fluctuation-dissipation theorem and linear response theory (Kubo et al., 1991), which explains equilibrium and near-equilibrium properties of a system with only a relaxation function (such as our $\Phi(t)$) and knowledge of a potential energy surface, such as that provided by our $g(\epsilon)$. Although the mathematics can be rather involved, especially with such broad relaxation functions as we have observed, several papers have elucidated the variety of effects that various $\Phi(t)$ can have on protein reactions (Onuchic, 1987; Rips and Jortner, 1987; Wang and Wolynes, 1994; Panchenko et al., 1995). The facts that we are observing energetic relaxation and that it is a long-range ET make it likely that our $\Phi(t, T)$ functions are sensitive to a wide variety of protein motions and so are a good choice for use in the absence of more specific information.

Relation to structure

The structural features responsible for the relaxation observed here can be identified by studying the influence of the environment on the relaxation, for example, by encasing it in PVA (Feher et al., 1987), dehydrating it (Clayton, 1978), or changing other factors such as solvent viscosity, pH, or type and concentration of salt in the solvent. Furthermore, the time and temperature dependence of the relaxation can be compared with that of specific reactions, for example, proton uptake, that have already been studied by other means in RCs (Maróti and Wraight, 1988; McPherson et al., 1988) or other proteins (vide infra).

Structural information can also be obtained by monitoring optical absorbance bands. Upon charge separation, electrochromic shifts are observed throughout the absorbance spectrum (Feher et al., 1987; Steffen et al., 1994), arising from the change in the electric field between the neutral and charge-separated states and the different dipole moments of the ground and excited states of each optical transition. We have measured shifts throughout the optical spectrum (350–950 nm) by cooling under illumination from 180 K. These shifts anneal on the same time scales as expected for CS1 and CS2 relaxations (unpublished observations). The shifts are in the direction opposite those caused by charge separation, suggesting that charge separation is followed by numerous changes that counteract the change in electric field. Therefore, we expect a correlation between the electrochromic shift of each absorbance band and ϵ and thus also the ET rate k. Indeed, Parot et al. (1987) have reported that $P^+Q_A^- \rightarrow PQ_A$ ET at 10 K occurs faster when measured on the blue side of the 804-nm BChl band than on the red. This is expected for a heterogeneous, static distribution of protein conformations, in which those CSs contributing to the blue edge of the 804-nm band undergo faster charge recombination than the average.

Several other groups have also observed complex wavelength dependences of ET rates in the near-IR bands. Kirmaier and Holten (1990) noted that the blue side of the 804-nm band also shows faster $P^* \rightarrow P^+H_A^-Q_A$ and $P^+H_A^-Q_A \rightarrow P^+H_AQ_A^-$ ET kinetics than the red side at both 285 K and 77 K. Sebban and Wraight (1989) observed faster ET kinetics of $P^+Q_A^- \rightarrow PQ_A$ on the blue side of the BChl band at 110 K and 295 K in *Rhodopseudomonas viridis* RCs, and on longer time scales than expected from the $\Phi(t, T)$ reported here. Tiede et al. (1996) investigated the temperature dependence of $P^+Q_A^-Q_B \rightarrow P^+Q_AQ_B^-$ ET by observing electrochromic shifts and reported spectroscopic evidence of conformational changes, but they were only able to investigate temperatures higher than those at which we expect the largest changes to be visible. Understanding the time and temperature dependence of protein relaxations will be essential in the investigation of the multitude of changes in the optical absorbance spectrum as various protein reactions are probed.

X-ray crystallography at cryogenic temperatures allows one, in principle, to obtain direct information on the structural changes. A crystal structure of RCs in the $P^+Q_A^-$ state has not yet been reported; however, a comparison of low-temperature (90 K) x-ray structures of RCs in the PQ_AQ_B and $P^+Q_AQ_B^-$ states has become available recently (Stowell et al., 1997). It shows significant structural changes. For example, in the charge-separated form, Q_B has moved 4.5 Å and undergone a propeller twist by 180°. Smaller changes were noted in nearby amino acids, but motions of protons and numerous other smaller changes throughout the protein that may contribute much of the energetic relaxation we observed are more difficult to characterize structurally.

Analogies have been drawn between proteins and glass-forming liquids because of similarities in their dynamics, such as large apparent Arrhenius activation energies, non-Arrhenius temperature dependence of the rates, and nonexponential time dependence of motions (Goldanskii et al., 1983; Iben et al., 1989; Parak and Nienhaus, 1991; Frauen-

felder et al., 1991; Young et al., 1991; Frauenfelder and Wolynes, 1994; Angell, 1995). These properties arise from the cooperative nature of structural rearrangements in these systems. For glass-forming liquids, a variety of physical explanations have been introduced, such as the free volume theory (Williams et al., 1955; Cohen and Turnbull, 1959), the entropy theory (Gibbs, 1956; Adam and Gibbs, 1965), and the mode coupling theory (Leutheusser, 1985; Bengtzelius et al., 1984). These theories are very different from one another, and none of them provides a microscopic picture that is valid for both the solid-like and fluid-like behaviors of viscous liquids. Goldstein (1969) and Stillinger (1995) have emphasized the idea that static and dynamic phenomena in glass-forming liquids can be modeled with a rugged potential energy landscape in a multidimensional configuration space, in which the glass transition occurs because the time for motions between energy minima crosses the experimental time scale. Ferry's Law (Eq. 22) was originally introduced as a phenomenological parameterization of the temperature dependence of motions in viscous liquids and polymers (Ferry et al., 1953), but can be obtained from a random walk of an excitation in a Gaussian density of states (Bässler, 1987; Zwanzig, 1988; Bryngelson and Wolynes, 1989).

Glycerol is a typical glass-forming liquid, and the cooperative motions in pure glycerol have been characterized over 13 orders of magnitude in time (200 ps to 2 ks) by dielectric relaxation spectroscopy (Dixon et al., 1990). Relaxation rates of the solvent used in our experiments (75% glycerol/25% water, v/v), measured by Huck et al. (1988), are similar and presented in the Arrhenius plot in Fig. 7.

A simple example illustrates how cooperative motions in our RC system can give rise to the anomalously high Arrhenius preexponentials and enthalpy barriers that we have observed. Consider the energetics of a proton migrating through the RC protein in response to Q_A^- formation. At high temperatures, the protein and solvent will be able to adapt to the moving point charge, presenting a partially solvated environment along the entire path. For the same proton transfer to occur in a frozen protein-solvent system, the proton will need to jump over much higher barriers. Consequently, two effects contribute to the increase in the rate as the temperature is raised. First, increased thermal energy makes it easier for the protein to reach activated states required for the conformational change. Second, the barriers to conformational change decrease as temperature increases, causing an additional speed-up in the rate with increasing temperature. Consequently, higher apparent activation enthalpies and preexponentials are obtained from the Arrhenius plot. Because the real enthalpy barriers only decrease over a limited range, the apparent enthalpy barriers will eventually decrease. The result is a curved Arrhenius plot (k versus $1/T$) with lower apparent barriers at higher temperatures, which can be approximated with Ferry's Law ($\log k \propto 1/T^2$).

Conformational substates in heme proteins

Much of the existing knowledge about structural heterogeneity and dynamics in proteins has been derived from studies of ligand binding to myoglobin (Mb) after flash photolysis, starting with the pioneering work by Frauenfelder and collaborators (Austin et al., 1975). This work led to a hierarchical model in which CSs are arranged in several tiers of substates (Frauenfelder et al., 1988, 1991; Nienhaus and Young, 1996; Nienhaus et al., 1997). The general features regarding the structure and dynamics of the energy landscape in myoglobin are similar to those observed here for RCs.

In carbonmonoxy myoglobin (MbCO), three "taxonomic" substates, called A substates (A_0, A_1, and A_3), can be distinguished by distinct infrared absorption bands of the bound CO. The temperature dependence of the interconversion rates, $A_0 \rightleftharpoons A_1 + A_3$ and $A_1 \rightleftharpoons A_3$, have been determined over the range from 10^{-6} s to 10^5 s (Johnson et al., 1996); these are shown in Fig. 7. The A substate exchange processes in myoglobin are seen to have activation enthalpies similar to those observed in the RC relaxation. Whereas the rates of the $A_0 \rightleftharpoons A_1 + A_3$ exchange agree with those in CS0 in RCs, the $A_1 \rightleftharpoons A_3$ exchange rates are faster, and so are more typical of CS1 in RCs. The $A_0 \rightleftharpoons A_1 + A_3$ exchange involves protonation/deprotonation of the imidazole side chain of H64 and local unfolding of the protein (Yang and Phillips, 1996; Müller et al., 1998). A recent discussion of structural and dynamic aspects of the A substates has been given by Johnson et al. (1996).

In MbCO, ligand recombination after flash photolysis between 60 and 160 K can be modeled with a distribution of activation enthalpy barriers, $g(H)$ (Austin et al., 1975; Steinbach et al., 1991), reflecting a heterogeneous ensemble of proteins. This observation corresponds to the presence of $g(\epsilon)$ distributions in RC samples. Agmon and Hopfield (1983) first showed that diffusion along parabolic surfaces (analogous to our Fig. 5) with a linear mapping of the conformational coordinate to the rebinding barrier H could explain ligand rebinding in the presence of relaxation. Steinbach et al. (1991) demonstrated that this relaxation was highly nonexponential in time, and low temperature illumination experiments by Chu et al. (1995) showed that changes in H can occur in large jumps, rather than in continuous shifts.

Myoglobin also shows motions below ~40 K that are similar to CS3 relaxations in RCs. They have been studied by spectral hole burning (Friedrich, 1995), low temperature specific heat measurements (Singh et al., 1984), and interconversion in the IR absorbance bands of the photodissociated CO (Mourant et al., 1993), and on shorter time scales by photon echo experiments (Thorn-Leeson and Wiersma, 1995).

X-ray structures of MbCO and the photoproduct Mb*CO that is generated by photodissociation at 20–40 K have characterized the changes that occur when motions in CS0,

CS1, and CS2 are arrested (Schlichting et al., 1994; Teng et al., 1994; Hartmann et al., 1996). Comparison of the photoproduct structure and the equilibrium unligated (deoxy) structure reveals the structural relaxations in the higher tiers of substates.

In both myoglobin and RC, thermally activated structural relaxations that inhibit the recombination reaction are observed on a wide variety of time scales. The similar relaxation behaviors of these two very different proteins suggest that the relaxation functions in Fig. 8 may apply to many different proteins. Although the barriers that oppose the relaxations are similar for both systems, the effect of relaxation on the reaction kinetics is quite different. CO recombination kinetics at 220 K extend from nanoseconds to seconds (Steinbach et al., 1991), whereas the $P^+Q_A^- \rightarrow PQ_A$ ET kinetics show a much smaller dispersion, ranging from tens to hundreds of milliseconds. This difference arises from the substantially different dependence of the reaction rate on the conformational coordinates: the CO recombination rate of myoglobin changes by many orders of magnitude as the molecule fluctuates among typical CSs, whereas the ET rate in RC changes by only a factor of $\sim$5. Because recombination in RCs takes $\sim$100 ms at all temperatures, we could unambiguously identify dynamic processes simply by cooling under illumination and observing as the protein anneals; the analogous experiment cannot be carried out in MbCO. In MbCO, the strong dependence of both relaxation and reaction rates on temperature leads to a very complex time and temperature dependence of the ligand binding reaction, making determination of $\Phi(t, T)$ for MbCO much more difficult.

CONCLUSIONS

Protein reactions require protein motions, so an understanding of these motions is required to understand protein reactions. In RCs, we have quantified the extent of conformational heterogeneity and observed that interconversion times between CSs are comparable to reaction times of many physiological reactions. To allow a concise description of the entire range of possible protein relaxation, it has been necessary to use a somewhat simplified model of electron transfer to explore the features of the energy landscape. Self-consistency between the regimes of static heterogeneity, relaxation, and fluctuation on time scales of ET and 10^5 times longer than the ET appeared naturally and explained several independent aspects of the data. We have compared our model to experiments designed to obtain the same information by independent means. We find agreement for both the dependence of the rate coefficient on the energy gap and temperature and for the time and temperature dependence of the relaxation function. The RC protein is one of many that use energetically favorable reactions to drive unfavorable ones. The present work clearly shows how long energy can be "extracted" from the nonequilibrium protein conformation (Fig. 8) as it occurs, for instance, in the protonation of amino acid residues.

The extrapolated room temperature relaxation function is smooth and continuous from picoseconds to milliseconds: on these time scales, sequential reactions occur in an ever-changing environment. Any reaction that is faster than the time scale of conformational changes will happen in a heterogeneous ensemble of proteins with a distribution of transition states. The special situation that allowed this study (the very weak dependence of rate on energy) is a rare exception. Most reactions are more like ligand binding to heme proteins, where the reaction rate is a much more sensitive function of protein conformation, and so the reaction rate will be more strongly influenced, or even determined, by the rate of conformational change of the protein.

We have studied the response of RCs to charge separation in both light- and dark-adapted conformations, and the ET could be observed in both conformations in the entire temperature range between 5 and 300 K. This allowed interpretation of the relaxation in terms of energy. It is possible to extend this study to different solvent conditions and to modified RC proteins, making it a useful probe of the effect of structural modifications on the energy landscape of RC. It also appears reasonable to use the relaxation functions presented here to help untangle the influence of conformational heterogeneity on the multitude of protein reactions in which it is less easy to isolate and characterize the effects.

This paper is dedicated to Prof. Hans Frauenfelder on the occasion of his 75th birthday.

We thank H. Frauenfelder, T. Gross, E. Takahashi, J. Wang, and P. G. Wolynes for helpful discussions.

This work was supported by the National Institutes of Health (grants PHS2 R01 GM 18051 and PHS5 T32 GM 08276) and the National Science Foundation (grants PHY95-13217 and IMCB 96-31063).

REFERENCES

Adam, G., and J. H. Gibbs. 1965. On the temperature dependence of cooperative relaxation properties in glass-forming liquids. *J. Chem. Phys.* 43:139–146.

Agmon, N., W. Doster, and F. Post. 1994. The transition from inhomogeneous to homogeneous kinetics in CO binding to myoglobin. *Biophys. J.* 66:1612–1622.

Agmon, N., and J. J. Hopfield. 1983. Transient kinetics of chemical reactions with bounded diffusion perpendicular to the reaction coordinate: intramolecular processes with slow conformational changes. *J. Chem. Phys.* 78:6947–6959.

Allen, J. P., G. Feher, T. O. Yeates, H. Komiya, and D. C. Rees. 1987. Structure of the reaction center from *Rhodobacter sphaeroides* R-26: the cofactors. *Proc. Natl. Acad. Sci. USA.* 84:5730–5734.

Angell, C. A. 1995. Formation of glasses from liquids and biopolymers. *Science.* 267:1924–1935.

Ansari, A., J. Berendzen, D. Braunstein, B. R. Cowen, H. Frauenfelder, M. K. Hong, I. E. T. Iben, J. B. Johnson, P. Ormos, T. B. Sauke, R. Scholl, A. Schulte, P. J. Steinbach, J. Vittitow, and R. D. Young. 1987. Rebinding and relaxation in the myoglobin pocket. *Biophys. Chem.* 26:337–355.

Ansari, A., C. M. Jones, E. R. Henry, J. Hofrichter, and W. A. Eaton. 1994. Conformational relaxation and ligand binding in myoglobin. *Biochemistry.* 33:5128–5145.

Arata, H., and W. W. Parson. 1981. Delayed fluorescence from *Rhodopseudomonas sphaeroides* reaction centers. Enthalpy and free energy changes accompanying electron transfer from P-870 to quinones. *Biochim. Biophys. Acta.* 638:201–209.

Atkins, P. W. 1990. Physical Chemistry, 4th Ed. W. H. Freeman and Co., New York. 850.

Austin, R. H., K. W. Beeson, L. Eisenstein, H. Frauenfelder, and I. C. Gunsalus. 1975. Dynamics of ligand binding to myoglobin. *Biochemistry.* 14:5355–5373.

Bässler, H. 1987. Viscous flow in supercooled liquids analyzed in terms of transport theory for random media with energetic disorder. *Phys. Rev. Lett.* 58:767–770.

Becker, M., V. Nagarajan, D. Middendorf, W. W. Parson, J. E. Martin, and R. E. Blankenship. 1991. Temperature dependence of the initial electron-transfer kinetics in photosynthetic reaction centers of *Chloroflexus aurantiacus. Biochim. Biophys. Acta.* 1057:299–312.

Beece, D., L. Eisenstein, H. Frauenfelder, D. Good, M. C. Marden, L. Reinisch, A. H. Reynolds, L. B. Sorensen, and K. T. Yue. 1980. Solvent viscosity and protein dynamics. *Biochemistry.* 19:5147–5157.

Bengtzelius, U., W. Götze, and A. Sjölander. 1984. Dynamics of supercooled liquids and the glass transition. *J. Phys. C Solid State Phys.* 17:5915–5934.

Beratan, D. N., J. N. Onuchic, and J. J. Hopfield. 1985. Limiting forms of the tunneling matrix element in the long distance bridge mediated electron transfer problem. *J. Chem. Phys.* 83:5325–5329.

Berendzen, J., H. Frauenfelder, T. Sauke, and R. Scholl. 1989. A logarithmic-timebase transient recorder. *Bull. Am. Phys. Soc.* 34:880a (Abstr.).

Bixon, M., J. Jortner, and M. E. Michel-Beyerle. 1995. A kinetic analysis of the primary charge separation in bacterial photosynthesis. Energy gaps and static heterogeneity. *Chem. Phys.* 197:389–404.

Bryngelson, J. D., and P. G. Wolynes. 1989. Intermediates and barrier crossing in a random energy model (with applications to protein folding). *J. Phys. Chem.* 93:6902–6915.

Chidsey, C. E. D., L. Takiff, R. A. Goldstein, and S. G. Boxer. 1985. Effect of magnetic fields on the triplet state lifetime in photosynthetic reaction centers: evidence for thermal repopulation of the initial radical pair. *Proc. Natl. Acad. Sci. USA.* 82:6850–6854.

Chu, K., R. M. Ernst, H. Frauenfelder, J. R. Mourant, G. U. Nienhaus, and R. Philipp. 1995. Light-induced and thermal relaxation in a protein. *Phys. Rev. Lett.* 74:2607–2610.

Clayton, R. K. 1978. Effects of dehydration on reaction centers from *Rhodopseudomonas sphaeroides. Biochim. Biophys. Acta.* 504:255–264.

Closs, G. L., and J. R. Miller. 1988. Intramolecular long-distance electron transfer in organic molecules. *Science.* 240:440–447.

Cohen, M. H., and D. Turnbull. 1959. Molecular transport in liquids and glasses. *J. Chem. Phys.* 31:1164–1169.

Dixon, P. K., L. Wu, S. R. Nagel, B. D. Williams, and J. P. Carini. 1990. Relaxation spectroscopies of viscous liquids. *Phys. Rev. Lett.* 65: 1108–1111.

Feher, G. and M. Y. Okamura. 1978. Chemical composition and properties of reaction centers. *In* The Photosynthetic Bacteria. R. K. Clayton and W. R. Sistrom, editors. Plenum Press, New York. 349–386.

Feher, G., M. Okamura, and D. Kleinfeld. 1987. Electron transfer reactions in bacterial photosynthesis: charge recombination kinetics as a structural probe. *In* Protein Structure: Molecular and Electronic Reactivity. R. Austin, E. Buhks, B. Chance, D. DeVault, P. L. Dutton, H. Frauenfelder, and V. I. Gol'danskii, editors. Springer Verlag, New York. 399–421.

Ferry, J. D., L. D. Grandine, Jr., and E. R. Fitzgerald. 1953. The relaxation distribution function of polyisobutylene in the transition from rubber-like to glass-like behavior. *J. Appl. Phys.* 24:911–916.

Franzen, S., and S. G. Boxer. 1993. Temperature dependence of the electric field modulation of electron transfer rates: charge recombination in photosynthetic reaction centers. *J. Phys. Chem.* 97:6304–6318.

Franzen, S., R. F. Goldstein, and S. G. Boxer. 1990. Electric field modulation of electron transfer reaction rates in isotropic systems: long-distance charge recombination in photosynthetic reaction centers. *J. Phys. Chem.* 94:5135–5149.

Frauenfelder, H., H. Hartmann, M. Karplus, I. D. Kuntz, Jr., J. Kuriyan, F. Parak, G. A. Petsko, D. Ringe, R. F. Tilton Jr., M. L. Connolly, and N. Max. 1987. Thermal expansion of a protein. *Biochemistry.* 26:254–261.

Frauenfelder, H., F. Parak, and R. D. Young. 1988. Conformational substates in proteins. *Annu. Rev. Biophys. Biophys. Chem.* 17:451–479.

Frauenfelder, H., G. A. Petsko, and D. Tsernoglou. 1979. Temperature-dependent x-ray diffraction as a probe of protein structural dynamics. *Nature.* 280:558–563.

Frauenfelder, H., S. G. Sligar, and P. G. Wolynes. 1991. The energy landscapes and motions of proteins. *Science.* 254:1598–1603.

Frauenfelder, H., and P. G. Wolynes. 1994. Biomolecules: where the physics of complexity and simplicity meet. *Phys. Today.* 47:58–64.

Friedrich, J. 1995. Hole burning spectroscopy and physics of proteins. *Methods Enzymol.* 246:226–259.

Garg, A., J. N. Onuchic, and V. Ambegaokar. 1985. Effect of friction on electron transfer in biomolecules. *J. Chem. Phys.* 83: 4491–4503.

Gibbs, J. H. 1956. Nature of the glass transition in polymers. *J. Chem. Phys.* 25:185–186.

Goldanskii, V. I., Yu. F. Krupyanskii, and V. N. Fleurov. 1983. Tunneling between quasi-degenerate conformational states and low-temperature heat capacity of biopolymers. The glasslike protein model. *Dokl. Biophys.* 272:209–212.

Goldstein, M. 1969. Viscous liquids and the glass transition: a potential energy barrier picture. *J. Chem. Phys.* 51:3728–3739.

Gopher, A., Y. Blatt, M. Schönfeld, M. Y. Okamura, G. Feher, and M. Montal. 1985. The effect of an applied electric field on the charge recombination kinetics in reaction centers reconstituted in planar lipid bilayers. *Biophys. J.* 48:311–320.

Green, J. L., J. Fan, and C. A. Angell. 1994. The protein-glass analogy: some insights from homopeptide comparisons. *J. Phys. Chem.* 98: 13780–13790.

Gunner, M. R., D. E. Robertson, and P. L. Dutton. 1986. Kinetic studies on the reaction center protein from *Rhodopseudomonas sphaeroides:* the temperature and free energy dependence of electron transfer between various quinones in the Q_A site and the oxidized bacteriochlorophyll dimer. *J. Phys. Chem.* 90:3783–3795.

Hartmann, H., F. Parak, W. Steigemann, G. A. Petsko, D. Ringe Ponzi, and H. Frauenfelder. 1982. Conformational substates in a protein: structure and dynamics of metmyoglobin at 80 K. *Proc. Natl. Acad. Sci. USA.* 79:4967–4971.

Hartmann, H., S. Zinser, P. Komninos, R. T. Schneider, G. U. Nienhaus, and F. Parak. 1996. X-ray structure determination of a metastable state of carbonmonoxy myoglobin after photodissociation. *Proc. Natl. Acad. Sci. USA.* 93:7013–7016.

Hopfield, J. J. 1974. Electron transfer between biological molecules by thermally activated tunneling. *Proc. Natl. Acad. Sci. USA.* 71: 3640–3644.

Huck, J. R., G. A. Noyel, and L. J. Jorat. 1988. Dielectric properties of supercooled glycerol-water solutions. *IEEE Trans. Elect. Insul.* 23: 627–638.

Iben, I. E. T., D. Braunstein, W. Doster, H. Frauenfelder, M. K. Hong, J. B. Johnson, S. Luck, P. Ormos, A. Schulte, P. J. Steinbach, A. H. Xie, and R. D. Young. 1989. Glassy behavior of a protein. *Phys. Rev. Lett.* 62:1916–1919.

Jackson, T. A., M. Lim, and P. A. Anfinrud. 1994. Complex nonexponential relaxation in myoglobin after photodissociation of MbCO: measurement and analysis from 2 ps to 56 μs. *Chem. Phys.* 180:131–140.

Johnson, J. B., D. C. Lamb, H. Frauenfelder, J. D. Müller, B. McMahon, G. U. Nienhaus, and R. D. Young. 1996. Ligand binding to heme proteins. VI. Interconversion of taxonomic substates in carbonmonoxymyoglobin. *Biophys. J.* 71:1563–1573.

Jortner, J. 1976. Temperature dependent activation energy for electron transfer between biological molecules. *J. Chem. Phys.* 64:4860–4867.

Kirmaier, C., and D. Holten. 1990. Evidence that a distribution of bacterial reaction centers underlies the temperature and detection-wavelength dependence of the rates of the primary electron-transfer reactions. *Proc. Natl. Acad. Sci. USA.* 87:3552–3556.

Kleinfeld, D., N. Okamura, and G. Feher. 1984. Electron-transfer kinetics in photosynthetic reaction centers cooled to cryogenic temperatures in the charge-separated state: evidence for light-induced structural changes. *Biochemistry.* 23:5780–5786.

Kubo, R., M. Toda, and N. Hashitsume. 1991. Statistical Physics II: Nonequilibrium Statistical Mechanics, 2nd Ed. Springer, New York.

Leggett, A. J., S. Chakravarty, A. T. Dorsey, M. P. A. Fisher, A. Garg, and W. Zwerger. 1987. Dynamics of the dissipative two-state system. *Rev. Mod. Phys.* 59:1–85.

Leutheusser, E. 1985. Dynamical model of the liquid-glass transition. *Phys. Rev. A* 29:2765–2773.

Levich, V. G., and R. R. Dogonadze. 1959. Teoriya bezizluchatelnikh electronnikh perekhodov mezhdu ionami v rastvorakh. *Dokl. Acad. Nauk. SSSR.* 124:123–126.

Lin, X., H. A. Murchison, V. Nagarajan, W. W. Parson, J. P. Allen, and J. C. Williams. 1994. Specific alteration of the oxidation potential of the electron donor in reaction centers from *Rhodobacter sphaeroides. Proc. Natl. Acad. Sci. USA.* 91:10265–10269.

Maróti, P., and C. A. Wraight. 1988. Flash-induced H^+ binding by bacterial photosynthetic reaction centers: influences of the redox states of the acceptor quinones and primary donor. *Biochim. Biophys. Acta.* 934: 329–347.

McPherson, P. H., M. Y. Okamura, and G. Feher. 1988. Light-induced proton uptake by photosynthetic reaction centers from *Rb. sphaeroides* R-26. I. Protonation of the one-electron states $D^+Q_A^-$, DQ_A^-, $D^+Q_AQ_B^-$, and $DQ_AQ_B^-$. *Biochim. Biophys. Acta.* 934:348–368.

Moser, C. C., J. M. Keske, K. Warncke, R. S. Farid, and P. L. Dutton. 1992. Nature of biological electron transfer. *Nature.* 355:796–802.

Mourant, J. R., D. P. Braunstein, K. Chu, H. Frauenfelder, G. U. Nienhaus, P. Ormos, and R. D. Young. 1993. Ligand binding to heme proteins. II. Transitions in the heme pocket of myoglobin. *Biophys. J.* 65: 1496–1507.

Nienhaus, G. U., J. R. Mourant, and H. Frauenfelder. 1992. Spectroscopic evidence for conformational relaxation in myoglobin. *Proc. Natl. Acad. Sci. USA.* 89:2902–2906.

Nienhaus, G. U., J. D. Müller, B. H. McMahon, and H. Frauenfelder. 1997. Exploring the conformational energy landscape of proteins. *Phys. D.* 107:297–311.

Nienhaus, G. U., and R. D. Young. 1996. Protein dynamics. *In* Encyclopedia of Applied Physics, Vol. 15. VCH Publishers, New York. 163–184.

Noks, P. P., E. P. Lukashev, A. A. Kononenko, P. S. Venediktov, and A. B. Rubin. 1977. Possible role of macromolecular components in functioning of photosynthetic reaction centers of purple bacteria. *Mol. Biol.* 11:835–842.

Ogrodnik, A., W. Keupp, M. Volk, G. Aumeier, and M. E. Michel-Beyerle. 1994. Inhomogeneity of radical-pair energies in photosynthetic reaction centers revealed by differences in recombination dynamics of $P^+H_A^-$ when detected in delayed emission and in absorption. *J. Phys. Chem.* 98:3432–3439.

Onuchic, J. N. 1987. Effect of friction on electron transfer: the two reaction coordinate case. *J. Chem. Phys.* 86:3925–3943.

Ortega, J. M., P. Mathis, J. C. Williams, and J. P. Allen. 1996. Temperature dependence of the reorganization energy for charge recombination in the reaction center from *Rhodobacter sphaeroides. Biochemistry.* 35: 3354–3361.

Panchenko, A. R., J. Wang, G. U. Nienhaus, and P. G. Wolynes. 1995. Analysis of ligand binding to heme proteins using a fluctuating path description. *J. Phys. Chem.* 99:9278–9282.

Parak, F., and G. U. Nienhaus. 1991. Glass-like behaviour of proteins as seen by Mössbauer spectroscopy. *J. Non-Cryst. Solids.* 131–133: 362–368.

Parot, P., J. Thiery, and A. Verméglio. 1987. Charge recombination at low temperature in photosynthetic bacteria reaction centers: evidence for two conformational states. *Biochim. Biophys. Acta.* 893:534–543.

Parson, W. W. 1967. Flash-induced absorbance changes in *Rhodospirillum rubrum* chromatophores. *Biochim. Biophys. Acta.* 131:154–172.

Peloquin, J. M., J. C. Williams, X. Lin, R. G. Alden, A. K. W. Taguchi, J. P. Allen, and N. W. Woodbury. 1994. Time-dependent thermodynamics during early electron transfer in reaction centers from *Rhodobacter sphaeroides. Biochemistry.* 33:8089–8100.

Popovic, Z. D., G. J. Kovacs, P. S. Vincett, G. Algria, and P. L. Dutton. 1986. Electric field dependence of recombination kinetics in reaction centers of photosynthetic bacteria. *Chem. Phys.* 110:227–237.

Rips, I., and J. Jortner. 1987. Dynamic solvent effects on outer-sphere electron transfer. *J. Chem. Phys.* 87:2090–2104.

Rubin, A. B., A. A. Kononenko, K. V. Shaitan, V. Z. Paschenko, and G. Yu. Riznichenko. 1994. Electron transport in photosynthesis. *Biofizika.* 39:173–195.

Sakurai, J. J. 1985. Modern Quantum Mechanics. Addison Wesley, New York. 104.

Schlichting, I., J. Berendzen, G. N. Phillips, Jr., and R. M. Sweet. 1994. Crystal structure of photolysed carbonmonoxy-myoglobin. *Nature.* 371: 808–812.

Schulten, K., and M. Tesch. 1991. Coupling of protein motion to electron transfer: molecular dynamics and stochastic quantum mechanics study of photosynthetic reaction centers. *Chem. Phys.* 158:421–446.

Sebban, P., and C. A. Wraight. 1989. Heterogeneity of the $P^+Q_A^-$ recombination kinetics in reaction centers from *Rhodopseudomonas viridis:* the effects of pH and temperature. *Biochim. Biophys. Acta.* 974:54–65.

Singh, G. P., H. J. Schink, H. von Löhneysen, F. Parak, and S. Hunklinger. 1984. Excitations in metmyoglobin crystals at low temperatures. *Z. Phys. B.* 55:23–26.

Skourtis, S. S., A. J. R. da Silva, W. Bialek, and J. N. Onuchic. 1992. A new look at the primary charge separation in bacterial photosynthesis. *J. Phys. Chem.* 96:8034–8041.

Steffen, M. A., K. Lao, and S. G. Boxer. 1994. Dielectric asymmetry in the photosynthetic reaction center. *Science.* 264:810–815.

Steinbach, P. J., A. Ansari, J. Berendzen, D. Braunstein, K. Chu, B. R. Cowen, D. Ehrenstein, H. Frauenfelder, J. B. Johnson, D. C. Lamb, S. Luck, J. R. Mourant, G. U. Nienhaus, P. Ormos, R. Philipp, A. Xie, and R. D. Young. 1991. Ligand binding to heme proteins: connection between dynamics and function. *Biochemistry.* 30:3988–4001.

Steinbach, P. J., K. Chu, H. Frauenfelder, J. B. Johnson, D. C. Lamb, G. U. Nienhaus, T. B. Sauke, and R. D. Young. 1992. Determination of rate distributions from kinetic experiments. *Biophys. J.* 61:235–245.

Stillinger, F. H. 1995. A topographic view of supercooled liquids and glass formation. *Science.* 267:1935–1939.

Stowell, M. H. B., T. M. McPhillips, D. C. Rees, S. M. Soltis, E. Abresch, and G. Feher. 1997. Light-induced structural changes in photosynthetic reaction center: implications for mechanism of electron-proton transfer. *Science.* 276:812–816.

Teng, T. Y., V. Srajer, and K. Moffat. 1994. Photolysis-induced structural changes in single crystals of carbonmonoxy myoglobin at 40 K. *Nature Struct. Biol.* 1:701–705.

Thorn-Leeson, D., and D. A. Wiersma. 1995. Looking into the energy landscape of myoglobin. *Nature Struct. Biol.* 2:848–851.

Tiede, D. M., J. Vázquez, J. Córdova, and P. A. Marone. 1996. Time-resolved electrochromism associated with the formation of quinone anions in the *Rhodobacter sphaeroides* R26 reaction center. *Biochemistry.* 35:10763–10775.

Treutlein, H., K. Schulten, A. T. Brünger, M. Karplus, J. Deisenhofer, and H. Michel. 1992. Chromophore-protein interactions and the function of the photosynthetic reaction center: a molecular dynamics study. *Proc. Natl. Acad. Sci. USA.* 89:75–79.

Wang, J., and P. G. Wolynes. 1994. Survival paths for reaction dynamics in fluctuating environments. *Chem. Phys.* 180:141–156.

Warshel, A., Z. T. Chu, and W. W. Parson. 1989. Dispersed polaron simulations of electron transfer in photosynthetic reaction centers. *Science.* 246:112–116.

Williams, M. L., R. F. Landel, and J. D. Ferry. 1955. The temperature dependence of relaxation mechanisms in amorphous polymers and other glass-forming liquids. *J. Am. Chem. Soc.* 77:3701–3707.

Woodbury, N. W., and W. W. Parson. 1986. Nanosecond fluorescence from chromatophores of *Rhodopseudomonas sphaeroides* and *Rhodospirillum rubrum. Biochim. Biophys. Acta.* 850:197–210.

Woodbury, N. W., S. Lin, X. Lin, J. M. Peloquin, A. K. W. Taguchi, J. A. C. Williams, and J. P. Allen. 1995. The role of reaction center excited state evolution during charge separation in a *Rb. sphaeroides* mutant with an initial electron donor midpoint potential 260 mV above wild type. *Chem. Phys.* 197:405–421.

Woodbury, N. W., J. M. Peloquin, R. G. Alden, X. Lin, S. Lin, A. K. W. Taguchi, J. C. Williams, and J. P. Allen. 1994. Relationship between

thermodynamics and mechanism during photoinduced charge separation in reaction centers from *Rhodobacter sphaeroides*. *Biochemistry*. 33: 8101–8112.

Xu, D., and K. Schulten. 1994. Coupling of protein motion to electron transfer in a photosynthetic reaction center: investigating the low temperature behavior in the framework of the spin-boson model. *Chem. Phys.* 182:91–117.

Yang, F., and G. N. Phillips, Jr. 1996. Structures of CO-, deoxy-, and metmyoglobins at various pH values. *J. Mol. Biol.* 256:762–774.

Young, R. D., H. Frauenfelder, J. B. Johnson, D. C. Lamb, G. U. Nienhaus, R. Philipp, and R. Scholl. 1991. Time and temperature dependence of large-scale conformational transitions in myoglobin. *Chem. Phys.* 158: 315–327.

Zollfrank, J., J. Friedrich, J. M. Vanderkooi, and J. Fidy. 1991. Conformational relaxation of a low-temperature protein as probed by photochemical hole burning: horseradish peroxidase. *Biophys. J.* 59:305–312.

Zwanzig, R. 1988. Diffusion in a rough potential. *Proc. Natl. Acad. Sci. USA.* 85:2029–2030.